1.

Paleoseismic record obtained by coring a lacustrine sag-pond along the North Anatolian Fault (Turkey)

Short title: Paleoseismological record of a sag-pond

A. Hubert-Ferrari[1], U. Avsar[2], M. El Ouahbi[1], G. Lepoint[1], N. Fagel[1]

1: University of Liege, Sart Tilman, B- 4000 Liège Belgium
2: Ghent University, Renard Centre of Marine Geology, Department of Geology and Soil Science, Krijgslaan 281 s.8, Gent 9000, Belgium

Complete Address of corresponding author:
A. Hubert-Ferrari: Unit 'Physical and Quaternary Géography', Department of Geography, University of Liege, Bat B11 - Sart Tilman, Allée du 6 aout 2, B- 4000 Liège Belgium, tel: +32-4366 93 95, email: aurelia.ferrari@ulg.ac.be

2. Subject Classification: 04.04.01 Earthquake geology and paleoseismology; 04.07.07. Tectonics

3. Abstract

Shallow lakes along minor structural bends or discontinuities of strike-slip fault are not usually paleoseismological target sites. In the present study we show that a 2m deep, 700m long lake crosscut by the North Anatolian Fault contain a reliable paleoseimological record obtain through coring. The North Anatolian Fault, a major strike-slip fault in Turkey last ruptured across the Asacipetecik Lake in 1939 with a slip of about 6 m. Seismic lines still shows remains of the fault ruptures forming minor 10 cm high scarps across the lake. Collected short cores show a set of sedimentary sequences composed of three different units. The lower unit, dark and fibrous, is similar to the present sedimentation at the top of the core. The strongly disturbed and whitish top unit 1 has anomalous organic matter content, grain size and mineralogy. The unit 2 is intermediate in between unit 1 and 3. The present stratigraphy is related to earthquake shaking inducing (1) sediment resuspension; (2) reworking of sediments coming from co-seismic scarps and lake margins; (3) increase in sedimentary runoff into the lake. The 2.5 m long core comprises 4 sequences, and thus 4 sedimentary events. Cesium and Lead data obtained in Boes *et al.* (2009) imply that Event 1 was triggered by the 1939 M=7.9 Erzincam Earthquake. Radiocarbon age dating suggest that Events 3 and 4 are initiated by the 1254 and the 1045 historical earthquake. Event 2 may correspond to the 1668 earthquake documented in paleoseimological trenches a few kilometers to the east.

4. Text of paper

1. Introduction

Obtaining a long paleoseimological record of strike-slip faults can be challenging because one needs a site where a continuous and slow trapping of sediments occurs. Key sites are thus often located along the fault structural discontinuities like pull-aparts and releasing bends present at different scale along strike-slip faults. These sites sedimentary traps have been

exploited to retrieve a continuous paleoseimological record along different strike-slip fault systems in the world (Weldon *et al.,* 2004; Kozaci *et al.,* 2011; Klinger *et al.*, 2003; Liu *et al.,* 2007). Some of these tectonic depressions can be underwater forming lakes, ponds or wetlands, and it is not possible to expose their sedimentary record in classical paleoseismological trenches (McCalpin, 2009). In the present study we show that an indirect paleoseismic record can still be obtained by coring.

Using sedimentary cores to retrieve a paleoseismological record is not straightforward because one can use only indirect sedimentological imprint of seismic shaking. Various studies have shown that they can be exploited to retrieve a long record of paleoearthquakes in lakes (eg. Schnellmann *et al.,* 2002; Becker *et al.,* 2005; Bertrand *et al.* 2007; Carrillo *et al.,* 2008; Beck 2009), in lagoons (Bertrand *et al.,* 2011), in small oceanic basins (eg. Gorsline *et al.,* 2000) and in oceans (Nakajima *et al.,* 2000; Goldfinger *et al.,* 2003, 2006, 2007; Beck *et al.* 2007). Earthquakes recorded in cores are usually identified as rapidly deposited layers intercalated within the more continuously and slowly depositing sedimentary sequence. Earthquakes can trigger a variety of different sedimentary processes that would let a specific imprint :(i) liquefaction, (ii) mass wasting flow and the associated deposition of turbidites; (iii) seiche motion (eg. the oscillation of the water body) and the induced resuspension of bottom lake sediments (Beck, 2009) ; (iv) change in the lake catchment related to coseismic weakening of substrate material and associated landslides which would trigger an increase in sediment delivery in the lake (Dadson *et al.,* 2004). The related abrupt changes in sediment texture and composition have been characterized using a wealth of different sedimentary proxies like magnetic properties (Larrosoana *et al.,* 2010; Beck, 2009), grain size (Shikia *et al.,* 2000; Bertrand *et al.,* 2007), geochemistry (Schwab *et al.,* 2009; Carrillo *et al.,* 2007), paleontological indicators (Cochran *et al.,* 2007; Hayward *et al.,* 2005; Leroy *et al.,* 2002, 2009; Schwab *et al.,* 2009), as well as high resolution seismic lines (Moernaut *et al.,* 2007, 2009) among others.

Most paleoseismological studies in lacustrine environments have focused on large lakes located in seismically active areas (eg. Monecke *et al.,* 2004; Moernaut *et al.,* 2007; Marco and Agno, 2005; Chaperon *et al.,* 1999) but off the fault zone. On the opposite, we present here the paleoseismological sedimentary record of a small and shallow pond, named the Asacitepecik Lake (AT Lake). The AT Lake occupied a small tectonic depression related to a minor releasing bend of a major strike-slip fault, the North Anatolian Fault. Our goal is to access the usefulness of such shallow structural lakes for paleoseismological studies.

In the present study, the morphology of the AT Lake and the fault scarps related to the 1939 earthquake rupture are documented combining sonar data and seismic data. The sedimentary infill of the AT Lake is sampled with sedimentary cores. Sudden textural and compositional changes in the retrieved sediments are studied combining X-ray imagery, magnetic susceptibility, mineralogy, Loss-On-Ignition (LOI), XRF geochemistry and carbon isotope analysis. The age of the sedimentary sequence is constrained combining radiocarbon age dating and previously published lead-cesium measurements (Boes *et al.,* 2009). Finally the possible link between sedimentary events and major historical earthquakes along the NAF are discussed and compared to nearby paleoseismological trench records.

2. Tectonic and Paleoseismological setting

Our study focuses on the North Anatolian Fault (NAF), a major, 1500 km long, right-lateral strike-slip fault in Turkey. The NAF accommodates, with its conjuguate the East Anatolian Fault, the westward motion of the Anatolian microplate away from the Arabia-Eurasia

collision zone (Hubert-Ferrari *et al.* 2002, Reilinger *et al.* 2006) (see inset in Figure 1). Along the NAF, the geological and geodetic slip rates are similar (eg. 20 to 25 mm/yr see Hubert-Ferrari *et al.* 2002, Kozaci *et al.* 2007; Reilinger *et al.* 2006) which suggest a simple seismic cycle characterized by nearly equal stress loading and strain release along this fault. The rupture of the NAF during the 20th century over 900 km further supported this view. The rupture occurred in a westward propagating sequence of M>7 earthquakes (Ambraseys 1970; Barka 1992) that started in 1939 in the east with the M=7.9 Erzincan earthquake and ended in the west with the 1999 Izmit and Duzce earthquakes (Stein *et al.* 1997; Hubert-Ferrari *et al.* 2000). The fault has also ruptured in sequence in the past (Ambraseys, 1977; 1988). However the integrated history of paleoearthquakes built using all paleoseismological data available along the NAF suggested variable reccurrence times along the fault linked to different tectonic regimes in the Anatolian microplate (Fraser *et al.,* 2010). The later implies a more complex seismic cycle than previously though.

In this paper we focus on the eastern NAF, which ruptured during the 1939 M=7.9 Erzincan Earthquake between Erzincan and Niksar (Figure 2). Published paleoseismological studies complied in Fraser (2010) suggest a complex history of ruptures along this segment dissimilar to the 1939 rupture. The 1939 earthquake broke three main fault segments comprising from east to west the 60 km long Erzincan, the 110 km long Mihar-Susheri and the 100 km Kelkit segments (Barka and Kadinsky-Cade, 1988; Barka 1996). This segmentation is based on the identification of major structural discontinuities. The earthquake slip in 1939 was variable along the different segments: irregular slip of 2 to 5 m occurred along the eastern Erzincan segment, high and consistent 5 to 7.5 m slip along the Mihar-Susheri segment and lower 4 to 3 m slip along the Kelkit segment (Barka, 1996).

Other large historical earthquakes took place along the eastern NAF in 1668, 1254, 1045 and 499 (Ambraseys 2009). Historical records of these earthquakes are sparse and incomplete, but paleoseismic studies detailed below allow a more accurate interpretation of the rupture extension of each earthquake. For the 1668 earthquake, damages are not well documented in the east with only the mention of some destruction in the towns of Erzincan and Tokat. Paleoseismic trenches along the Kelkit and the Susheri segments (numbers 1-2-3 in Figure 1; Fraser *et al.,* 2010; Zabci *et al.,* 2011; Fraser *et al.,* this volume) document a fault rupture at that time, but paleoseismic studies (number 4 in Figure 1; Hartleb *et al.,* 2006; Kozaci *et al.,* 2011) further east documented no major earthquake from the 14th to 19th centuries. About the 1254 earthquake, Ambraseys and Melville (1995) as well as Ambraseys and Jackson (1998) reported historical surface ruptures from Erzincan to Susheri, and paleoseismic trenches along all segments (numbers 1 to 4 in Figure 1) document an earthquake during that time period. Historical account damages related to the 1045 earthquake are centered in Erzincan, and trenches along the Erzincan segment (numbers 4 and 2 in Figure 1) documented a paleoearthquake during that time period. In 499, large destructions occurred in the towns of Niksar (eg. NeoCaesare), Susheri (e.g. Nicopolis) as well as strong disturbances of the Euphratus River near Erzincan (Ambraseys 1995). The 499 earthquake is documented in all paleoseismic trenches along the eastern NAF. Paleoseismic data thus suggest a rupture pattern along the eastern NAF that could be irregular (Fraser *et al.,* 2010b). The sedimentological study of the Asacitepecik Lake infill along the central Susheri-Mihar segments seeks to provide additional paleoseismological constraints within this franework.

3. Site Description

3.1. Local Tectonics and Paleoseismologial records

The Asacitepecik lake (AT Lake) is located in the Golova Basin infilled with Pliocene conglomerates with some alternating shale and marl deposits (Kocyigit 1990). The basin fill rest on a basement formed of different units. To the north along at the basin margin outcrop Permian and Triassic schist and marble units; to the south lie the Ophiolitic mélange linked to the Ankara-Erzincan tethyan suture and the associated tertiary clastic and carbonate sediments (Kocyigit, 1990).

The Golova Basin is 3 km wide and 35 km lomg with a strike similar to the NAF, and is presently bordered by weakly active normal faults and crosses cut by the N110^{o} striking Mihar-Susheri segment. In its central part the Cobanli river has an apparent right-lateral offset of 7 to 15 km depending onto interpretation (Barka and Kadinsky-Cade 1988; Kocyigit, 1990). The basin morphology is linked to the right-lateral motion along the NAF, which occurred since Mio-Pliocene time (Kocyigit, 1990) and looks like an evolved crosscut pull-apart basin similar to the Hazar Lake along the East Anatolian Fault (Garcia-Moreno *et al.,* 2010). Across the basin, small-scale structural complexities outcrop along the Mihar-Susheri segment, one of them being the small depression occupied by the studied AT Lake. The 1939 fault rupture mapped by Kocyigit (1990) and Barka (1996) indeed runs across the AT Lake and a coseismic slip of 6.5 m deduced from the offset of field boundaries was documented few 100s m west of the Lake

Several paleoseismic trenches were excavated near the AT Lake. The trench of Zabci *et al.* (2008) is located just a few 100's m west of the AT Lake (40.0402N/ 38.5800E). Stratification and clear structural relations indicate three events including 1939 Erzincan one, but the ages of the determined paleo-events could be constrained due to limited samples for radiocarbon age dating (Zabci, personal communication). The exploratory trench of Okomura *et al.* (1994) (40.046111°N / 38.562222°E) is located 2 km west of the Lake, but no detail information is available about the trench study. About 2 to 4 km east of the AT Lake, Fraser *et al.* (this volume) have opened a series of three trenches (T1 : 40.028226°N/ 38.617813°E ; T2 : 40.026173°N/ 38.623918°E ; T3 : 40.021265°N/ 38.638594°E). The paleoseismic investigation defined the timing of six paleoearthquakes, four corresponding to historical earthquakes (Event 0: 1939; Event 1: 1668; Event 2: 1254; Event 3: 499). However this investigation was plagued by poor dating results and an anomalously large number of radiocarbon dates were excluded from the OxCal analysis by the authors.

3.2. Local Geomorphology

The geomorphology around the AT Lake is shaped both by the flow of Cobanli River and by right-lateral deformation along the North Anatolian Fault (Figure 2). To the south of the NAF, the northward flowing Cobanli River forms a wide alluvial plain, but to the north the river bends easward and have a narrow meandering bed. The AT Lake is located just at the northward limit of the wide alluvial plain, about 700 m west from the present Cobanli riverbed (Figure 2). In fact an elongated ridge standing 25 m above the riverbed separates the AT lake from the Cobanli riverbed. The later ridge as well as the depression occupied by the AT lake are interpreted as related to minor steps or bends along the NAF (Figures 2 and 3).

The tectonic depression occupied by the AT Lake is 700m long and 200m wide and elongated along the NAF fault (Figure 3). The lake has no catchment and is surrounded by low hills with very gentle slopes. Its maximum water depth is about 2 m, and the lakeshore are filled with vegetation (e.g. Phragmites). On the eastern and northeastern shallow shores, there are geomorpholgical indications of former higher paleoshorelines (See white arrows in Figure 3).

Along its southern edge, A small village occupies a local high and man-made channels used for irrigation have been built. All lands around the lake are agricultural fields.

3.3. Lake preliminary sedimentological study

A preliminary sedimentological study of the AT Lake was conducted by Boes *et al.* (2009). In this paper, a short core of the AT lake is studied as well as four others coming from different lakes along the NAF. In all the cores the sedimentological fingerprints of the 20th century earthquake sequence were identified using excess 210Pb and 137Cs measurements. In the AT Lake, the sedimentary disturbance associated with the M=7.9 1939 earthquake is identified at depths between 10 and 55 cm, and possibly down to 99 cm; in addition a mean sedimentation rate of 1.5 mm/year over the last 70 years was inferred (Boes *et al.*, 2009). Finaly this study conclude that the AT Lake do record past major earthquakes rupturing the NAF.

4. Materials and Methods

4.1. Bathymetry, geophysics and coring

Given that no previous information was available on the AT Lake, we produced a bathymetric map using a Garmin GPS map 178 equipped with a sonar in 2006 (Figure 3). In addition to clarify the interplay between the NAF structure and the lacustrine sedimentation, eight single channel seismic reflection profiles were acquired in 2007 with an Innomar SES2000-Compact Sub-bottom Profiler (ITU-EMCOL equipment) in the deepest western part of the Lake. Both the primary High Frequency signal (100 kHz) and the secondary Low Frequency signal (6 to 12 kHz) were recorded. Penetration reached 50cm to 1m using the LF signal and 1 to 3 m using the HF signal.

Sedimentary cores were collected in 2006 and 2007 within the framework of the Seismic Cycle project (Hubert-Ferrari, 2007). In 2006, the 1.2 m long short core labeled AT003 partly studied in Boes *et al.* (2010) was retrieved from the central part of the Lake (N40.03924; E38.58752, depth: 1.9 m) using a modified UWITEC gravity corer. In 2007, we collected a 2.6 m long piston core labeled AT2007 and an associated 1 m long gravity core labeled AT2007-SC (N40.03876 E38,58836) slightly more to the east. The present paper is based on the analysis of all cores with a special focus on the longest core, AT2007.

4.2 Sediment analysis

Different types of analysis were performed on the cores to characterize both the background continuous sedimentation and significant rapidly deposited layer potentially related to earthquakes. To characterize abrupt sedimentological changes in the cores, we first did a detailed visual stratigraphic log of all the cores (somewhat similar to conventional paleoseismic trench logging) that we complemented by smear slides of the different sedimentary fractions (>450μm, 450-250μm, 250-100μm). Stratigraphy and microstructures were further investigated using X-ray imagery on the AT2007 core (SCOPIX system EPOC Bordeaux I, France; see Migeon *et al.* 1998) and textural properties examined with individual granulometric analyses on the AT2007-SC core (Malvern Mastersizer). Before grain-size measurements, organic matter was digested using hot H_2O_2.

Sedimentological changes recorded in the AT lake were further probed using magnetic susceptibility data acquired on all cores at 5 mm resolution using the Geotek multi-sensor core logger of Rhodes Island University (USA). The magnetic susceptibility data and the macroscopic descriptions were used to correlate the different cores (Figure 4). To constrain any compositional change associated with sedimentary event we perform bulk mineralogy

analyses using X-ray diffraction (XRD) on 80 samples of the AT2007 core. To investigate organic matter changes in the AT pond colonized by phragmites, we combine Loss-on-ignition data (4h at 550° ; 135 measurements) with measurements of Total Organic Carbon (TOC), Carbon/Nitrogen (C/N) ratios, carbon and nitrogene stable isotopes (60 samples treated with HCl to removed all mineral carbonates before the analysis) on the AT2007 core.

Finally to better decipher the origin of the sudden sedimentary changes in the cores, measurement of major elements (Al, Si, S, Cl, K, Ca, Ti, Mn, Fe, Rh) were undertaken on the AT2007 core by X-ray-fluorescence (XRF) analysis at 0.5 cm resolution (10 kV, 2mm spacing on the Avaatech core scanner of EPOC Bordeaux I, France). XRF core-scanner data are only semi-quantitative measurement of element abundance (Croudace *et al.,* 2006; Richter *et al.,* 2006; Rothwell and Rack, 2006), because of variable water content, grain-size distribution, inhomogeneity of the specimens, and the irregular scanned surface of a core. Part of these problems can be overcome using ratio of elements, which are thus considered as more reliable proxy. Here we present Ca and Ti counts data, as well as Ca/Ti ratio (Figure 8) that we compare to other analysis to assess the significance of the XRF data obtained.

4.3 Dating

The age of the sedimentary record was constrained using AMS radiocarbon age dating. Nine bulk samples were first selected. Given the poor results, seeds were then hand picked in the AT2007 core in the >450 μm fraction for the analysis. Results are presented in Table 1. Ages were calibrated with OxCal 4.0 using the IntCal04 atmospheric curve of Reimer *et al.* [2004].

5. Results

5.1. Local Fault structure in and around AT Lake

The bathymetry map in Figure 4 shows that the AT lake is very shallow reaching a maximum water depth of about 2 m (Figure 3). The depression occupied by the AT Lake is divided in two parts: a shallow marsh in the west and a deeper basin in the east. The deep basin lies north of the AT village, in straight continuity with the main fault exposed in the paleoseismological trench of Zabci *et al.* (2008).

The seismic imaging is poor, probably because the organic rich sediments of the AT Lake are degraded and are converted to methane. The gas charged sediments prevent any imaging below 2.5 m (Figure 4). The Low Frequency profiles still clearly imaged the lake bottom showing a northern steeply deeping slope, a more gentle southern slope, a nearly flat depression in between, and several scarps. Two main fault scarps (>10 cm) labeled F1 and F2 offset the deep flat basin and the other minor scarps (≤ 10 cm) affect the southern slope. All scarps can be consistently followed in the different profiles. The F1 scarp always shows a downthrown block to the south consistent with minor normal faulting on this fault, and F2 scarp shows variable geometries consistent with strike-slip faulting. Minor scarps affecting the southern edge of the AT lake might be related to normal faulting or to mass movement. The High Frequency profiles suggest larger 40 to 55 cm high vertical cumulative offsets at a depth of 2 m below the surface scarps F1 and F2 (Figure 4b). The F1-F2 fault system is in straight continuity with the onland fault trace trenched by Zabci *et al.* (2008), and can be interpreted as the principal displacement zone across the AT Lake. The fault structure is similar to flower structure with the right-lateral motion on F2 and normal faulting on F1, associated with extensional faulting along the lake southern edge.

5.2 Cores sediment characteristics

The main results of the multi-proxy analyses are presented in the Fig. 5, 6 , 7 and 8.

5.2.1. Stratigraphy and Core Correlation based on Magnetic susceptibility measuerements and X-Ray imagery

The three cores AT003, AT2007-SC, AT2007 show fine organic rich sediments. The MS values of the sediments are generally low below 5, which correspond to the range of paramagnetic material expected in carbonate, organic rich sediments. The stratigraphy of the three cores is similar. Each core shows alternating packages of dark brown fibrous organic-rich silty clays and lighter brown to whitish silty clays with a minor sandy fraction labelled here "sequences". The top of all core is a dark-brown fibrous package, quiet homogeneous with thicknesses between 16 to 23 cm that we labelled sequence 0. Below the top sequence 0 there are two sequences in AT2007-SC, three in AT003-2006, and four in AT2007; each sequence comprises at the bottom a dark fibrous layer similar to the top sediment and at the top a light color layer. Individual sequences can be correlated in between the different cores because they have similar visual and magnetic susceptibility characteristics. Futhermore each sequence was subdivided in three sedimentary units labeled 1 to 3 for respectively the top, middle and unit bottom one. This subdivision is based on differences in (1) natural and X-Ray gray scale color, (2) apparent textural organization of their organic content, (3) structural characteristics (disturbance, laminations, etc.). A detailed description of each unit is given below. It is mostly based on the long core AT-2007 for which we have a high quality detailed X-Ray image.

The bottom unit 3 in most sequences is a fibrous dark color silty clay unit similar to the topmost unit (sequence 0) with a rare mineral fraction. It shows variable thickness ranging from 15 cm in sequence 1 to 75 cm in sequence 3. The unit is composed of fibrous plant remains mostly phragmites binding silty-clay aggregates (Figure 7c). The organic fibers are mostly intact and form a closed spaced net filled with silt and clay. Visual inspection of the unit shows a general homogeneity with some gradual changes. The X-Ray pictures are generally dark and homogeneous also suggesting an opaque and dense material. The general characteristics of unit 3 described above are applicable to all sequences with minor differences between the AT003 core and the AT2007 and AT2007-SC cores. In the later, fibers are oriented perpendicular to the water-sediment interface, implying in place growth at shallow water depth and progressive sedimentary burial. In AT003 core, fibrous materials are organized in lamina, and the sedimentation is characterized by alternating organic and terrigenous lamina (Boes *et al.,* 2009). This difference may reflect the deeper water range at the site of AT003 than at site of cores AT-2007. Similar laminated sediments are observed at the bottom of core AT-2007 in unit 3 of the sequence 4.

The top unit 1 in all sequences is a light color sandy silty clay unit, rich in mixed organic materials. It shows similar thickness ranging from 14 to 18 cm. The main general characteristics of unit 1 are its strong heterogeneity with repeated marked stratigraphic variations associated with visible disturbances. In addition X-Ray pictures are lighter than in unit 3 suggesting a more transparent and less dense material. The top part of all units 1 is marked by whitish layer with a strong concentration small black phragmite seeds (Figure 6) and overlies lamina of different thicknesses, colors and apparent textures. The whitish layers in the sequences 1 and 2 form key stratigraphic markers identifiable in the different 3 cores and show low MS values. Finally in the X-ray imagery, particular sedimentary structures are observed. In the unit 1 of sequence 1, there are strongly contrasted flaser bedding-like structures similar to coastal tidal bedding. These structures indicate oscillating currents during deposition and have been interpreted as related to earthquake-triggered seiche effects (see Beck *et al.,* 2007). In sequence 2, the unit 1 is strongly disrupted with discontinuous and disrupted lamina, wavy contacts in between lamina, and small-scale liquefactions. In

sequence 3, the whole 25 cm thick unit 1 is strongly disturbed with no throughgoing horizontal lamina which contrasts with the underlying unit. In sequence 4, the 10 cm thick unit 1 is just structureless and no lamina are observed.

The middle unit 2 in all sequences in core AT2007 shows a gradual transition to units 1 and 3, and similar thicknesses ranging from 3.5 cm to 10 cm. The color and visual characteristics of unit 2 are intermediate in between units 1 and 3. The unit is usually rich in phragmite fibers like unit 3, but heterogeneous, with strong disturbances like in unit 1. Fragmite fibers are organized in lamina which gave wavy contacts, inequal thicknesses and frequent disruptions.

5.2.2. Grain size

Grain size of the mineral fraction analyzed in AT2007-SC comprise on average 85% silt, 10% clay, 5% sand particules. A significant part of the sand and silt particules are in fact composed of clay aggregates and ostracods. The grain size distribution show significant variations. A marked global increase in grain size occurs in the units 1 of sequences 1 and 2. In any unit 1, we also identify small scale grain-size variations related to the different lamina forming the unit. In addition the maximum in sand grain size does not occures at the exact same location in sequence 1 and 2. In sequence 1, a maximum of sand is reached at the topmost part of unit 1 and a maximum in clay content above at the bottom of sequence 0. In sequence 2, the maximum in grain size is reached in the middle of the unit and the proportion sand size particles decreased sharply in the top whitish subunit and clay reaches a local maximum at the transition to upper sequence 1.

5.2.3. Mineralogy

The sediments have a unusual mineralogy summarized below giving average values with minima and maxima observed. The minerals identified include quartz (mean:5%; min:1%; max: 9%), calcite with a significant fraction of high-Mg calcite (mean:7%; min:2%; max:11%) with a significant percent of Mg rich calcite, dolomite (mean:7%; min:4%; max:10%), clay (mean:51%; min:41%; max:70%), plagioclase (mean:5%; min:0%; max:17%), hematite (mean:4%; min:0%; max:9%), goethite (mean:13%; min:0%; max:22%), hydromagnesite (mean:5%; min:0%; max:13%). There is also a variable quantity of aragonite (0 to 20%) that we choose to exclude from the quantification.

The lacustrine mineralogy is unusual with up to 40% of iron oxides (hematite and goethite) and Ca-Mg carbonates (calcite, dolomite and hydromagnesite). In particular hydromagnesite is observed. Hydromagnesite is a rare evaporitic hydrocarbonate mineral ($Mg_5(CO_3)_4(OH)_2.4(H_2O)$) and its occurence implies that the lake is supersaturated with respect to Mg and has a high total alkalinity and a ph greater than 9. To crystallize hydromagnesite directly from lake water, the Mg over Ca ratio must be very high (>500) and the Mg concentration above 34g/l (Müller *et al.,* 1972). Hydromagnesite has been documented in the sediments of few lakes around the world. Those lakes are characterized by an arid climate like the ephemeral lakes in Southern Australia (Van Der Borch, 1965) or the Lake Siling in central Tibet (Goto *et al.,* 2003) or by magnesium rich ultramafic host-rock like the wetland of Altin in British Columbia (Power *et al.,* 2007) or by a combination of both like for the Lake Salda in Southern Turkey (Braithwaite and Zedef, 1994). For the AT Lake, the supersaturation in magnesium may be reached through intense evaporation of its shallow water during summer months, but to reach the level required for the precipitation of hydromagnesite, there must be some significant Mg input from the catchment or from groundwater. In the Golova Basin, the part of the basement rock is an ophiolitique complex naturally rich in magnesium which erosion produced the sedimentary rocks surrounding the

lake. The fact that we also have a high content in iron oxides in the AT sediments could also be linked to iron-bearing source rocks found in ophiolite complex and to the resulting iron-enriched topsoils surrounding the lake. Finally in most lakes and wetland around the world, the precipitation of hydromagnesite is catalyzed by cyanobacteria (Wright 1999; Braithwaite and Zedef 1996; Power *et al.,* 2007). In that case hydromagnesite can precipitate with a lower concentration and a lower Mg:Ca ratio (Power *et al.,* 2007). We infer that it is also true for the AT Lake.

In Figure 8 we present a cumulative diagram of the iron oxides (hematite+goethite), plagioglase plus quartz, Mg-carbonates (dolomite+hydromagnesite) and calcite excluding clays. The complete mineralogical data with clay is presented in the appendix. Quartz and plagioclase (qz+plg) have the similar downcore evolution and are presented together. Calcite has a trend similar to quartz and plagioclase, and opposite to iron oxydes and Mg-carbonates. The opposite trend of calcite and dolomite is expected as high-Mg calcite can react with lake water having an Mg/Ca ratio greater than seven to form dolomite (Müller *et al.,* 1972). Quartz and Plagioclase have high relative aboundance from the depth of 250 cm at the core bottom (sequence 4-unit 3) to the depth of 155cm (top of sequence 3-unit 3). At shallower depths their proportion decrease. Local maxima and minima are reached in lamina in unit 1 in sequence 1. Iron oxides and Mg-carbonates have relative low proportion from the core bottom to the depth of 150 cm and higher proportion at shallower depth. The maximum aboundances in Mg-carbonates are systematically reached in units 1, and local minima in the units 3. The typical whitish color of unit 1 may be linked to a greater proportion of hydromagnetite, a white mineral.

5.2.4. XRF Geochemical variation

The intensity of all major elements measured (Ca, Fe, Si, Mn, Ti, Al, K) is positively correlated. Titatium and calcium intensities are presented in Figure 8. The Ti element was choosen because it is not affected by early diagenesis and because it is usually interpreted like Fe, Si, Mn, Al, K as representing the siliciclastic terrigeneous input from the lake catchment and shores. The Ca element on the opposite is often interpreted as an indicator of biogenic productivity.

The Ti-XRF curve shows large variations similar to the magnetic susceptibility measurements. Ti abundance decreases from the core bottom upward to reach minima at depth of 150 cm (top unit 3-sequence 3) and at 120 cm (units 1-2 in sequence 3). At shallower depths, Ti intensity shows small scale variations without any global trend. There are systematic local minima at the top of all units 1. We also note that the Ti-XRF variations are roughly similar to quartz-plagioclase changes determined through XRD (Figure 8).
The changes in Ca intensities are very similar to Ti intensities (Figure 8) and to Calcite changes determined through XRD. The coeval evolution of Ti and Ca elements are also clearly illustrated using the Ti/Ca ratio presented in Figure 8. The nearly constant Ti/Ca ratio suggests a strong link between productivity and nutrient input associated with the siliciclastic sediments. There are still marked sudden increases in Ti over Ca ratio mostly in units 2 in sequences 1 to 3 and a boarder increase in unit 3 in sequence 3.

5.2.4. Organic Matter: LOI, TOC, δ13C and smear slides

The loss-on ignition data at 550 ^{o}C presented in figure 9 show a mean organic content of 35% with strong variations in between the different units. In particular the units 3 in sequences 2, 3 and 4 have relative low organic content (30%) whereas units 1 or 2 in all sequences show relative maxima with up to 65% of organic matter. In addition we observe a

gradual increase in organic matter in unit 3 in sequence 3 from 25% at 208cm depth to 35% at 150 cm depth; above there is a stronger step increase with about 60%.

Smear slides of the different sieved fraction in units 1 to 3 help characterizing the coarse (>100μm) material present in the sediments and particularly the different types of organic materials. The content of the different units differs significantly but all contains phytoclasts and silty-clay aggregates forming soft grains of different sizes.
In units 3, the dominant fraction is usually greater than 450μm and composed of elongated fibers of phragmites. **In units 1**, there is a greater diversity of materials and marked changes in organic content through each individual layer, except for unit 1 in sequence 4 which is quiet homogeneous. For example the whitish top of the unit 1 in sequence 1 has its primary fraction smaller than 450μm and is composed in the 250-450 μm fraction of ostracod shells and of 60% seeds most of which being black phragmite seeds (see photos in Figure 6). The high concentration of these black seeds is also visible by eyes in units 1 in sequence 1, 2 (see Figure 6) and 4 (see Figure 9b). In the fraction greater than 450 μm different types of seeds are also present; in the 100-250 μm fraction 60% is composed of broken ostracod shells. In the same unit 1, the laminas below the whitish layer present a different content. The fraction >450 μm is more abundant with large seeds, some chironomids and different types of plant remains; the 250-450 μm fraction shows a mixture of broken ostracod shells in less amount than the layer above, chironomids, seeds, phytoclasts, amorphous silty-clay organic aggregates; the 100-250 μm fraction shows broken ostracoda but again in less amount than above and amorphous silty-clay organic aggregates. **Units 2** is intermediate between units 1 and 2, with a high variability, a relative abundance of ostracods like unit 1, and in the fractions >250 μm elongated fibrous plant remains mostly absent in units 1. It also contains some beds with more clastic sediments.

The TOC data display variations somewhat similar to LOI (550^{o}C) data but much smoother. Its general trend is described below. From the core bottom to a depth of 115 cm in unit 1 in sequence 3, there is a general slow increase with a local peak in the unit 1 in sequence 4. The increase is followed by a general minor decrease to the depth of 75 cm in the middle of unit 1 in sequence 2. At shallower levels TOC data show a set of strong and rapid variations with two maxima in the units 1 of sequences 1 and 2 and minima in the unit 3 in sequence 1.

C/N ratio is fairly constant oscillating around a mean value of 11 with a standard deviation of 1. The ratio is slightly higher (11.6±0.9) in the lower part of the core until a depth of 125 cm (the top of unit 2-sequence 3) than in the shallower part of the core (10.4±0.8). The unchanging C/N reflects a constant ratio between terrestrial and aquatic sources for the organic matter supplied to the AT lake (Meyers and Teranes, 2001).

The $\delta^{13}C$ data follow a similar trend without marked peak. The low values (-24.5‰) at the core bottom increasing to a maximum (-18‰) at depth of about 125 cm (unit 2-sequence 3), then $\delta^{13}C$ curve shows a decreasing trend to minima (-22‰) around 60 cm (unit 1-sequence 2; unit 3- sequence 1), at shallower depth the $\delta^{13}C$ value increases slightly and show minor variations around the mean values of -19‰ to -20‰. Though carbon stable isotopes have similar isotopic values for both the terrestrial and aquatic organic sources, the fact that we do have a constant C/N ratio suggest that changes in $\delta^{13}C$ are triggered by changes in productivity in the aquatic organic source. An increased productivity can yield to an increase in $\delta^{13}C$ of organic matter that is produced in the lake and is available for sedimentation (Meyers and Teranes, 2001). Variability in aquatic species can also triggered an increase in

$\delta^{13}C$, specially a relative increase in cyanobacteria species, which have usually high carbon stable isotopic values (Vuorio *et al.,* 2006).

The $\delta^{15}N$ data show a trend quiet opposite to the $\delta^{13}C$. From the core bottom, the $\delta^{15}N$ value decrease and reach a minimum (2‰) at 110cm depth. At shallower depth in sequence 2, $\delta^{15}N$ reaches maxima of 10 ‰ which suggests that denitrification occurred at that time (Hoefs, 2009); it decreases sharply in sequence 1 and reaches minima of 2.6‰.

5.3 . Dating

Lead and Cesium data from the AT003 core and published in Boes et al. (2009) implies that the unit 1 in sequence 1 is related to the 1939 earthquake, which rupture crosses the AT Lake. This unit is thus interpreted as a seismite of the 1939 earthquake. The timing of the sequence 4 and the lower part of sequence 3 are constrained using radiocarbon age dating on seeds. Sequence 4 was deposited between 780 AD and 1020 AD and sequence 3 from 1040 AD to at least 1220 AD. The record of core AT 2007 spans about 1100 years.

6. Interpretation

6.1. Event stratigraphy

We interpret the sedimentary record in the long AT2007 core as well as in the associated short cores to reflect repeatedly earthquake disturbed sedimentation. The unit 1 in sequence 1 is identified as a rapid deposited layer triggered by the 1939 fault rupture crossing the lake. In particular the flaser beds at the base of unit 1 would be linked to seiche motion. The other disturbed and heterogeneous units 1 would also represent earthquake triggered sedimentary deposits; the bases of these units are thus considered to be event horizons.

A specific imprint of M>7 earthquakes in the AT lake is expected for several reasons. Seismic shaking and the triggered water mass oscillation would erode the lake subaqueous marginal slopes, rework the upper unconsolidated water-saturated sedimentary layer. A large amount resuspended sediments would thus settle progressively. Fault rupture across the lake would create scarps which collapse would bring further materials into the lake. Finally in the catchment, slope failure on the subaerial gentle slopes and loosen soil material would result in an increase of the sedimentary run-off into the lake. The observed stratigraphy with three distinctive units would represent for unit 3 an undisturbed “normal” sedimentation, for unit 2 a disturbed in-situ sedimentary layer, and for unit 1 a mixed anomalous sedimentary unit composed of remobilized lacustrine sediments and of sediments coming from the catchment. The characteristics of the 3 units resumed below fit the present interpretation.

The dark fibrous unit 3 of variable thickness presents an undisturbed net of vertical organic fibers filled with silty-clay aggregates identical to the present background sedimentation documented at the top of the core. Sedimentary changes are gradual without large disturbances. This organic sedimentation occurs naturally in the shallow depth near shore environment of the AT lake colonized with phragmites.
The intermediate unit 2 has organic characteristics similar to the unit 3, but it is strongly disturbed with phragmite fibers forming lamina. Unit 2 has also an anomalous Ti/Ca ratio indicating a higher concentration in heavy clastic terrigenous particules, which would occur if denser particules were concentrated in that layer. It would be derived from the top unit 3 and represent the non-resuspended sedimentary layer at the lake bottom during the earthquake from which part of the sediments have been extracted and resuspended during shaking.
The top unit 1 is anomalous units regarding its structural organization, grain size, organic content and mineralogy. Strong disturbances are visible comprising structureless layers,

small-scale liquefactions, flaser-bedding structures and disrupted or wavy lamina. Grain-size of the non-organic fraction show an increase in sand particles. Unit 1 has also the highest organic content, but is distinctive from units 2 and 3 because it lacks phragmite fibers. Instead it contains varied seeds, ostracod shells and phytoclasts. Because the C/N data indicates no significant change in the balance between aquatic and terrestrial input, most of the organic matter must be reworked during earthquake shaking. In fact after an earthquake, the light and unbounded elements (eg. seeds, phytoclasts and ostracods) would concentrate in the triggered resuspension and be deposited according to their settlement velocity. This interpretation is in agreement with the fact that we have at the top of unit 1 the greatest amount of ostracods and an increase in the aboundance of hydromagnesite, which have a low density (hydromagnesite density: 2.25 g/cm3). This process alone cannot fully account for the particular mineralogy of unit 1. In particular the coeval increase in Mg-carbonates and iron oxides can only be explain by an increase of allochtonous Fe and Mg bearing elements into the lake. These elements would come from the enhanced erosion of topsoils surrounding the lake triggered by earthquake shaking. Finally the generally complex stratigraphy of unit 1 composed of several layers or lamina could be linked to complex and variable balance between terrigenous input and resuspension. Various resuspension episodes can be triggered by large M≥6 aftershooks. Variable terrigenous inputs would also occur at different time period depending onto its origin: slope failure on the lake margin, collapse of fault scarps or sedimentary runoff following large rainfalls.

6.2. Chronology

The AT 2007 core has four units 1 which bases are event horizons. Event 1 forming the unit 1 in sequence 1 is related to the 1939 earthquake rupture crossing the AT Lake. The timing of the two bottom events 3 (unit 1-sequence 3) and 4 (unit 1-sequence 4) is constrained using radiocarbon age dating on large seeds and an ordering Bayesian model similar to the one used in nearby trenches (Fraser *et al.,* this volume). Five samples are used in the model and one sample is excluded and interpreted as reworked. In the model (Figure 10) the bottom event 4 occurred between 982AD and 1091AD (including 1 sigma uncertainties) and event 3 occurred after 1216AD. The age of event 2 (unit 1-sequence 2) is unconstrained.

The dating of the sedimentary events is compatible with historical seismicity. The 1939 Erzincan earthquake triggered event 1. Event 4, which age is constrained between 982AD and 1091AD, is compatible with the occurrence of the 1045 historical event, and event 3, which occurred after 1216AD, may correspond with the 1254 earthquake. Finally event 2 which age is not constrained could match the 1668 earthquakes. The later would impy a reccurrence rate of about 300 years on the eastern NAF at the Asacitepecik site.

6.3. Other environmental changes recorded

Independently of the earthquake-induced units 1 and the earthquake-disturbed unit 2, the cores shows some gradual sedimentary changes that reflect limnological changes related to local or more global environmental changes. A major gradual change occurs from the lake bottom (250 cm) to the top of unit 3 in sequence 3 at a depth of 135 cm characterized: (1) an increase in organic matter, iron oxides and Mg-Carbonates; (2) a decrease in plagioclase, quartz, calcite and Ti. We interpret these changes to be related to a decrease in the water level increasing the colonization of near shore plant and the magnesium and iron concentration in the water. This interpretation is compatible with higher lake levels indentified around the lake (Figure 3). This evolution might be related to an increase in evaporation during summer months and a decrease in precipitation during the winter months, which would correspond to a global increase in aridity. The observed changes in organic matter elemental and isotopic

compositions can also be related to water depth changes. In particular Sifeddine *et al.* (2011) has shown in a shallow lake in Venezuela that TOC concentrations, $\delta^{13}C$ values increase and $\delta^{15}N$ values decrease in the transverse transects as water depth decreases from 4 m to 0 m. At depths shallower than 110 cm, we see the opposite pattern in core AT2007 with a local minimum in TOC-$\delta^{13}C$, iron oxides and Mg-carbonates at 50-60 cm in unit 3 in sequence 1 which would suggest a slight depth water increase.

7. Discussion

7.1. Origin of the events identified

Sedimentary events in lakes can be triggered by a variety of natural causes other than earthquakes. Considering the present setting of the AT Lake, at least two main forcing agents can be identified: storms and droughts. Strong storms would have high wind speed, which would induce sediment resuspension and increase sedimentary run-off in the lake. This process can account for most of the observed disturbances, the anomalous organic content of unit 1, but not for the iron oxide and Mg-carbonate anomalies. On the opposite, significant drought would decrease sharply the lake- level, concentrate Mg and Fe elements in the lake water and increase the precipitation of Mg-carbonates and iron oxides, but not induced the sedimentary disruptions observed. Furthermore the average recurrence rate of events in the AT Lake is about 300 years, which is too long compare to the usual return period of strong storms and droughts. Finally the occurrence of the earthquake-related sedimentary events in the AT Lake fully agrees with historical seismicity in the area. We thus believe that the sedimentary events observed in the AT lake are uniquely generated by earthquakes, which is the only agent capable of producing the variety of anomalies observed.

7.2. Comparison with respect to other paleoseismological studies

The inferred paleoearthquakes recorded in the AT lake are the 1939, 1668, 1254 and 1045 historical earthquakes. This record does not fully match the paleoseismological data obtained from trenches located a few kilometers east of the AT Lake (Fraser *et al.,* this volume). The first four paleoearthquakes identified in Fraser *et al.* (this volume) have ages and would match the 1939, 1668, 1254 and 499 historical earthquakes; our event 4 attributed to the 1045 earthquake near the base of the core is thus not recorded in theses trenches. Other paleoseimological trenches located 65 km east of the AT lake (Hartleb *et al.,* 2006; Kozaci *et al.,* 2011) along the Erzincan segment do record the 1045 earthquake, which destroyed the Erzincan city (Guidoboni and Comastri 2005). Trenches located 110 km to the west of the AT lake near Resadiye also record an earthquake between A.D. 991 and 1078 with 68.2% probability which is interpreted to be the 1045 earthquake (Zabci *et al.,* 2010). The fact that the 1045 earthquake was not recorded in the trenches of Frasers *et al.* (this volume) could be thus be related to an incomplete record. However event 4 in the AT Lake can also be a far-field effect of the 1045 Erzincan Earthquake. If the later event did break the Erzincan segment but not the Mihar-Susheri segment, the earthquake shaking would still be strong enough to trigger most of the sedimentary anomalies associated to event 4. We would need more paleoseismological data to confirm or not the rupture along Mihar-Susheri segment during the 1045 earthquake.

8. Conclusion

The AT Lake occupying a small tectonic depression along the eastern NAF contains a reliable record of paleoearthquakes. The earthquake sedimentary imprints are intercalated in the normal fibrous rich lacustrine sedimentation. They have particular anomalous mineralogical, organic, textural and structural signatures. The anomalies are interpreted to result from (1) resuspension; (2) reworking of sediments coming from coseismic scarps and lake margins; (3)

increase in sedimentary runoff into the lake. Four events are identified. Event 1 corresponds to the 1939 earthquake which rupture is still visible in seismic profiles across the lake. Event 3 and 4 which ages are constrained using radiocarbon age dating would correspond to the 1254 and 1045 historical events. Event 2 is inferred to match with the 1668 earthquake. A comparison with nearby paleoseimological trenches points to the difficulty in lakes in differencing the effect of an earthquake rupturing through the studied lake and the far field effects of major earthquakes occurring on nearby fault segments.

5. Data and sharing sources

The satellite images in figures 2 and 3 are Google Earth imagery.

6. Acknowledgements

This work was carried out in the frame of the Marie Curie Excellence Grant Project "Understanding the irregularity of seismic cycles: A case study in Turkey" (MEXT-CT-2005-025617: Seismic Cycles) centered at the Seismology Section of the Royal Observatory of Belgium whom we would like to thank for their support. We are grateful for the assistance of Prof. Erhan Altunel of Osmangazi University for assistance with logistics. The seismic lines and the AT2007 cores was retrieved thanks to a fruitfull collaboration with EMCOL (Eastern Mediterranean Centre for Oceanography and Limnology) and its director Namik Cagatay.

7. References

Ambraseys, N. (2009). Earthquakes in the Mediterranean and Middle East - A Multidisciplinary Study of Seismicity up to 1900, Cambridge University Press, pp.968.

Ambraseys, N.N. and C.P. Melville (1995). Historical evidence of faulting in eastern Anatolia and northern Syria, Annali di Geofisica, 38, 337–343.

Ambraseys, N.N. and C.F. Finkel (1995). The Seismicity of Turkey and adjacent areas: a historical review, 1500–1800, Istanbul, Muhittin Salih Eren.

Ambraseys, N.N. and J.A. Jackson (1998). Faulting associated with historical and recent earthquakes in the eastern Mediterranean region, Geophysical Journal International, 133, 390–406.

Ambraseys, N.N. and C.F. Finkel (1988). The Anatolian earthquake of 17 August 1668, in Historical Seismograms and Earthquakes of the World, W. H. K. Lee, H. Meyers, and K. Shimazaki (Editors), Academic, San Diego, Calif., 173 – 180.

Ambraseys, N.N. (1970). Some characteristic features of the North Anatolian Fault Zone, Tectonophysics 9, 143–165.

Barka, A.A. and K. Kadinsky-Cade (1988). Strike-slip fault geometry in Turkey and its influence on earthquake activity, Tectonics, 7, 663-684.

Barka, A. A. (1992). The North Anatolian fault zone, Annales Tectonicae, 164-195.

Barka, A.A., (1996). Slip distribution along the North Anatolian Fault associated with the large earthquakes of the period 1939 to 1967, Bull. Seismol. Soc. Am., 86, 1238–1254.

Becker, A., M. Ferry, M. Schnellmann and D. Giardini (2005). Multiarchive palæoseismic record of late Pleistocene strong earthquakes in Switzerland, Tectonophysics, 400, 153–157.

Beck, C., B. Mercier de Lépinay, J.-L. Schneider, M. Cremer, N. Çağatay, E. Wendenbaum, S. Boutareaud, G. Ménot, S. Schmidt, O. Weber, K. Eris, R. Armijo, B. Meyer, N. Pondard, M.-A. Gutscher, and the MARMACORE Cruise Party, J.-L. Turon, L. Labeyrie, E. Cortijo, Y. Gallet, H. Bouquerel, N. Gorur, A. Gervais, M.-H. Castera, L. Londeix, A. de Rességuier, A. Jaouen, (2007). Late Quaternary co-seismic sedimentation in the Sea of Marmara's deep basins, in Sedimentary Records of Catastrophic Events, F. Bourrouilh-Le Jan, C. Beck, D. Gorsline (Editors.), Spec. Issue Sedimentary Geology, 199, 65–89.

Beck, C. (2009). Late Quaternary lacustrine paleo-seismic archives in north-western Alps: Examples of earthquake-origin assessment of sedimentary disturbances, Earth-Science Reviews, 96, 327-344.

Bertrand, S., F. Charlet, E. Chapron, N. Fagel and M. De Batist (2007). Reconstruction of the Holocene seismotectonic activity of the Southern Andes from seismites recorded in Lago Icalma, Chile, 39°S, Palaeogeography, Palaeoclimatology, Palaeoecology, 259, 301-322.

Bertrand, S., M. Sterken, L. Vargas-Ramirez, M. De Batist, W. Vyverman, G. Lepoint and N. Fagel (2009). Bulk organic geochemistry of sediments from Puyehue Lake and its watershed (Chile, 40°S): Implications for paleoenvironmental reconstructions, Palaeogeography, Palaeoclimatology, Palaeoecology, 294, 56-71. doi:10.1016/j.palaeo.2009.03.012

Bertrand, S., L. Doner, S. Akçer Ön, U. Sancar, U. Schudack, S. Mischke, N. Çagatay and S.A.G. Leroy. (2011). Sedimentary record of coseismic subsidence in Hersek coastal lagoon (Izmit Bay, Turkey) and the late Holocene activity of the North Anatolian Fault, Geochem. Geophys. Geosyst., 12, Q06002, doi:10.1029/2011GC003511.

Boes, X., S.B. Moran, J. King, M.N. Cagata, and A. Hubert-Ferrari. (2009). Records of large earthquakes in lake sediments along the North Anatolian Fault, Turkey, Paleolimnol DOI 10.1007/s10933-009-9376-x

Braithwaite, C. and V. Zedef (1994). Living hydromagnesite stromatolites from Turkey, Sedimentary Geology 92, doi:10.1016/0037-0738(94)90051-5

Braithwaite, C. and V. Zedef (1996). Hydromagnesite Stromatolites and Sediments in an Alkaline Lake, Salda Golu, Turkey, Journal of Sedimentary Research, 66, doi: 10.1306/D426845F-2B26-11D7-8648000102C1865D.

Carrillo, E., C. Beck, F. Audemard, E. Moreno and R. Ollarves (2008). Disentangling Late Quaternary climatic and seismo-tectonic controls on Lake Mucubaji sedimentation (Merida Andes, Venezuela), Palaeogeography, Palaeoclimatology, Palaeoecology, 259, 284-300.

Chapron, E., C. Beck, M. Pourchet and J-F. Deconinck (1999). 1822 earthquake-triggered homogenite in Lake Le Bourget (NW Alps), Terra Nova, 11, 86-92.

Cochran, U., M. Hannah, M. Harper, R. Van Dissen, K. Berryman and J. Begg (2007). Detection of large, Holocene earthquakes using diatom analysis of coastal sedimentary sequences, Wellington, New Zealand, Quaternary Science Reviews, 26, 1129-1147, ISSN 0277-3791, doi: 10.1016/ j.quascirev.2007.01.008.

Croudace, I.W., A. Rindby and R.G. Rothwell (2006). ITRAX: description and evaluation of a new multi-function X-ray core scanner. In: Rothwell, R.G. (Ed.), New Techniques in Sediment Core Analysis. Special Publication 267, Geological Society, London, 51–63.

Dadson, S.J., N. Hovius, H. Chen, W. B. Dade, J.-C. Lin, M.-L. Hsu, C.-W. Lin,

M.-J. Horng, T.-C. Chen, J. Milliman, C.P. Stark (2004). Earthquake-triggered increase in sediment delivery from an active mountain belt, Geology, 32, 733–736.

Fraser, J. G., J.S. Pigati, A. Hubert-Ferrari, K. Vanneste, U. Avsar and S. Altinok (2009). A 3000-year record of ground-rupturing earthquakes along the central North Anatolian Fault near Lake Ladik, Turkey, Bulletin of the Seismological Society of America, 99, 2681-2703, doi:10.1785/0120080024.

Fraser, J., A. Hubert-Ferrari, K. Vanneste, S. Altinok and L. Drab (2010a). A relict paleoseismic record of seven earthquakes between 2000 B.C. and 600 A.D. on the central North Anatolian Fault at Elmacik, near Osmancik, Turkey, Geological Society of America Bulletin, 122, 1830-1845.

Fraser, J., K. Vanneste and A. Hubert-Ferrari (2010b), Recent behavior of the North Anatolian Fault: Insights from an integrated paleoseismological data set, J. Geophys. Res., 115, doi:10.1029/2009JB006982.

Garcia Moreno, D., A. Hubert-Ferrari, J. Moernaut, J. Fraser, X. Boes, M. Van Daele, M. De Batist, E. Damci and N. Cagatay (2009). Structure and evolution of Lake Hazar pull-apart Basin along the East Anatolian Fault, Basin Research, 23, 191–207.

Goldfinger, C., C.H. Nelson and J.E. Johnson (2003). Holocene earthquake records from the cascadia subduction zone and northern San Andreas Fault based on precise dating of offshore turbidites, Annual Review of Earth and Planetary Sciences, 31, 2003, 555-577.

Goldfinger, C., A. Morey and H. Nelson (2006). Deep-water turbidites as Holocene earthquake proxies along the Northern San Andreas Fault system, Seismol. Res. Lett., 77, 195–196.

Goldfinger, C., A. Morey, C. Nelson, J. Gutierrez-Pastor, J. Johnson, E. Karabanov, J. Chaytor and A. Eriksson (2007). Shipboard Scientific Party, Rupture lengths and temporal history of significant earthquakes on the offshore and north coast segments of the Northern San Andreas Fault based on turbidite stratigraphy, Earth and Planetary Science Letters, 254, 9-27.

Gorsline, D.S., T. De Diego and E.H. Nava-Sanchez (2000). Seismically triggered turbidites in small margin basins : Alfonso Basin, western Gulf of California and Santa Monica Basin, California Borderland, Sediment. Geol., 135, 21-35.

Goto, A., H. Arakawaa, H. Morinagaa and T. Sakiyamab (2003). The occurrence of hydromagnesite in bottom sediments from Lake Siling, central Tibet: implications for the correlation among d 18O, d 13C and particle density, Journal of Asian Earth Sciences, 21, 979–988.

Guidoboni, E., A. Comastri and G. Traina (1994). Catalogue of Ancient Earthquakes in the Mediterranean Area up to the 10th Century. ING-SGA, Bologna.

Hartleb, R., D. Dolan, J.F. Kozaci, H.S. Akyuz and G.G. Seitz (2006). A 2500-yr-long paleoseismologic record of large, infrequent earthquakes on the North Anatolian fault at Cukurcimen, Turkey, Bulletin of the Geological Society of America, 118, 823-840, doi:810.1130/B25838.25831.

Hayward, B., H. Grenfell, A. Sabaa, R. Carter, U. Cochran, J. Lipps, P. Shane and M. Morley (2005). Micropaleontological evidence of large earthquakes in the past 7200 years in southern Hawke's Bay, New Zealand, Quaternary Science Reviews, 25, 1186-1207, ISSN 0277-3791, doi: 10.1016/ j.quascirev.2005.10.013.

Hoefs, J. (2009) Stable Isotope Geochemistry, Springer, pp. 197.

Hubert-Ferrari, A., R. Armijo, B. Meyer, G.C.P. King and A. Barka (2002). Morphology, displacement and slip rates along the North Antolian Fault (Turkey), Journal of Geophysical Research, 107, 10.1029/2001JB000393.

Hubert-Ferrari, A., A. Barka, E. Jacques, S. Nalbant, B. Meyer, R. Armijo, P. Tapponnier and G.C.P. King (2000). Seismic hazard in the Sea of Marmata following the Izmit Earthquake, Nature, 404, 269-273.

Hubert-Ferrari A., X. Boes, J. Fraser, U. Avsar, K. Vanneste, N. Cagatay, E. Altunel, M. de Batist and N. Fagel (2007). Understanding the irregularity of Seismic cycles: A Case study in Turkey-A Marie Curie Excellence Team Project, European Geosciences Union Meeting, Geophysical Research Abstract, 9, 06720. Poster.

Klinger, Y., K. Sieh, E. Altunel, A. Akoglu, A. Barka, T. Dawson, T. Gonzales, A. Meltzner and T. Rockwell (2003). Paleoseismic evidence of characteristic slip on the western segment of the North Anatolian fault, Turkey. Bull. Seis. Soc. Am., 93, 2317 – 2332.

Koçyig ̆it, A., (1990). Tectonic setting of the Gölova basin, total offset of the North Anatolian Fault Zone, Eastern Pontide, Turkey, Annales Tecton., 4, 155–170.

Kozacı, O., J.F. Dolan, R.C. Finkel and R.D. Hartleb (2007). Late Holocene slip rate for the North Anatolian fault, Turkey, from cosmo- genic 36Cl geochronology: Implications for the constancy of fault loading and strain release rates, Geology, 35, 867–870, doi:10.1130/ G23187A.1.

Kozaci, O., J. Dolan, O. Yönlü and R. Hartleb (2011). Paleoseismologic evidence for the relatively regular recurrence of infrequent, large-magnitude earthquakes on the eastern North Anatolian fault at Yaylabeli, Turkey, Lithosphere, 3, 37-54, doi: 10.1130/L118.1

Larrasoana, J., M. Ortuno, H. Birks, B. Valero-Garces, J. Pares, R. Copons, L. Camarero and J. Bordonau (2010). Palaeoenvironmental and palaeoseismic implications of a 3700-year sedimentary record from proglacial Lake Barrancs (Maladeta Massif, Central Pyrenees, Spain), Palaeogeography, Palaeoclimatology, Palaeoecology, 294, 83-93, ISSN 0031-0182, DOI: 10.1016/j.palaeo.2009.04.003.

Leroy, S., S. Boyraz and A. Gurbuz (2009). High-resolution palynological analysis in Lake Sapanca as a tool to detect recent earthquakes on the North Anatolian Fault, Quaternary Science Reviews, 28, 2616-2632, ISSN 0277-3791, DOI: 10.1016/j.quascirev.2009.05.018.

Leroy, S., N. Kazanci, O. Ileri, M. Kibar, O. Emre, E. McGee and H.I. Griffiths (2002). Abrupt environmental changes within a late Holocene lacustrine sequence south of the Marmara Sea (Lake Manyas, N-W Turkey): possible links with seismic events, Marine Geology 190, 531-552, ISSN 0025-3227, doi: 10.1016/S0025-3227(02)00361-4.

Liu, J., Y. Klinger, X. Xu, C. Lasserre, G. Chen, W. Chen and P. Tapponnier (2007). Millenial recurrence of large earthquakes on the Haiyuan fault near Songshan, Gansu province, China, Bull. Seis. Soc. Am., 97, 14-34.

Marco, S. and A. Agnon (2005). High-resolution stratigraphy reveals repeated earthquake faulting in the Masada Fault Zone, Dead Sea Transform, Tectonophysics, 408, 101–112.

McCalpin, J. (2009). Paleoseismology Academic Press - Nature – pp. 613.

Meyers, P.A. and J.L. Teranes (2001). Sediment organic matter. In: Last, W.M., Smol, J.P. (Eds.), Tracking Environmental Changes Using Lake Sediment —. Physical and geochemical methods, vol. 2. Kluwer Academic, Dordrecht, The Netherlands, pp. 239–270.

Migeon, S., O. Weber, J. Faugeres and J. Saint-Paul (1999). SCOPIX : a new X-ray imaging system for core analysis, Geo-Marine Letters, 18, 251–255.

Moernaut, J., M. De Batist, F. Charlet, K. Heirman, E. Chapron, M. Pino, R. Brümmer and R. Urrutia (2007). Giant earthquakes in South-Central Chile revealed by Holocene mass-wasting events in Lake Puyehue, Sedimentary Geology, 195, 239–256.

Moernaut, J., M. De Batist, K. Heirman, M. Van Daele, M. Pino, R. Brümmer and R. Urrutia (2009). Fluidization of buried mass-wasting deposits in lake sediments and its relevance for paleoseismology: Results from a reaction seismic study of lakes Villarrica and Calafquén (South-Central Chile), Sedimentary Geology, 213, 121–135.

Monecke, K., F.S. Anselmetti, A. Becker, M. Sturm and D. Giardini (2004). The record of historic earthquakes in lake sediments of Central Switzerland, Tectonophysics, 394, 21-40.

Müller, G., G. Irion, U. Forstner (1972). Formation and diagenesis of inorganic Ca–Mg carbonates in the lacustrine environment. Natürwissenschaften 59, 158–164.

Nakajima,T. and Y. Kanai (2000). Sedimentary features of seismoturbidites triggered by the 1983 and older historical earthquakes in the eastern margin of the Japan Sea, Sedimentary Geology, 135, 1-19, DOI: 10.1016/S0037-0738(00)00059-2.

Okomura, K., T. Yoshioka and I. Kusçu (1994). Surface faulting on the North Anatolian Fault in these two millennia, Proceedings of the workshop on paleoseismology, Open-File Report 94-568, USGS, p. 143-144.

Power, I., S. Wilson, J. Thom, G. Dipple and G. Southam (2007). Biologically induced mineralization of dypingite by cyanobacteria from an alkaline wetland near Atlin, British Columbia, Canada, Geochemical Transactions, 8, doi:10.1186/1467-4866-8-13.

Reilinger, R., *et al*. (2006). GPS constraints on continental deformation in the Africa-Arabia-Eurasia continental collision zone and implications for the dynamics of plate interactions, J. Geophys. Res., 111, B05411, doi:10.1029/2005JB004051.

Richter, T.O., S. Van der Gaast, B. Koster, A. Vaars, R. Gieles, H. De Stigter, H. De Haas and T.C.E. van Weering (2006). The Avaatech XRF core scanner: technical description and applications to NE Atlantic sediments. In: Rothwell, R.G. (Ed.), New Techniques in Sediment Core Analysis. Special Publication 267. Geological Society, London, 39–50.

Rothwell, R.G. and F.R. Rack (2006). New techniques in sediment core analysis: an introduction. In: Rothwell, R.G. (Ed.), New Techniques in Sediment Core Analysis. Special Publication 267. Geological Society, London, 1–29.

Schwab, M., P. Werner, P. Dulski, E. McGee, N. Nowaczyk, S. Bertrand and S. Leroy (2009). Palaeolimnology of Lake Sapanca and identification of historic earthquake signals, Northern Anatolian Fault Zone (Turkey), Quaternary Science Reviews, 28, 991-1005.

Sifeddine, A., P.M. Meyers, R.C. Cordeiro, A. Luiza, S. Albuquerque, M. Bernardes, B. Turcq and J.J. Abrao (2011). Delivery and deposition of organic matter in surface sediments of Lagoa do Cacço (Brazil), J Paleolimnol, 45:385–396 DOI 10.1007/s10933-011-9506-0.

Stein, R.S., A.A. Barka and J.H. Dieterich (1997). Progressive failure on the North Anatolian fault since earthquake stress triggering, Geophys. J. Inter. 128, 594–604.

Schnellmann, M., F.S. Anselmetti, D. Giardini, J.A. McKenzie and S. Ward (2002). Prehistoric earthquake history revealed by lacustrine slump deposits, Geology, 30, 1131-1134.

Shikia, T., F. Kumonb, Y. Inouchic, Y. Kontanid, T. Sakamotoe, M. Tateishif, H. Matsubarag and K. Fukuyamah (2000). Sedimentary features of the seismo-turbidites, Lake Biwa, Japan, Sedimentary Geology, 135, 37-50.

Van Der Borch, C. (1965). The distribution and preliminary geochemistry of modern carbonate sediments of the Coorong area, South Australia, Geohimica et Cosmochimica Acta, 29, 781-799.

Weldon, R. J., K.M. Scharer, T.E. Fumal and G.P. Biasi (2004). Wrightwood and the earthquake cycle: what a long recurrence record tells us about how faults work, GSA Today, 14, 4-10.

Zabci, C., V. Karabacak, T. Sancar, H.S. Akyuz, E. Altunel, H. Gursoy and O. Tatar (2008), The possible eastward continuation of the 17 August 1668 Anatolian Earthquake on the North Anatolian Fault (NAF), Turkey, Geophysical Research Abstracts 10, EGU2008-A-05542.

Zabci, C., H.S. Akyuz, V. Karabacak, T. Sancar, E. Altunel, H. Gursoy and O. Tatar (2010). Paleoearthquakes on the Kelkit Valley Segment of the North Anatolian Fault, Turkey: Implications for the Surface Rupture of the Historical 17 August 1668 Anatolian Earthquake, Turkish Journal of Earth Sciences, 20, 411-427.

8. Table

Table 1. Radiocarbon age dating from AT2007 core

Label	Depth (cm)	Width (cm)	Description	Yield	mg	$d^{13}C$	Fc	+/-	^{14}C age	+/-
AT2007/01 0-100 36-37	36.5	0,5	Bulk sediment	3,8%	1,09	-27,3	0,7249	0,0038	2580	40
AT2007/01 0-100 56-57	56.5	0,5	Bulk sediment	3,7%	1,17	-30,5	0,6922	0,0026	2960	30
AT2007/01 0-100 80-81	80.5	0,5	Bulk sediment	5,0%	1,32	-26,9	0,7723	0,0037	2080	40
AT2007/01 100-200 33-34	133.5	0,5	Bulk sediment	5,9%	1,08	-23,5	0,7834	0,0028	1960	30
AT2007/01 100-200 85-86	185.5	0,5	Bulk sediment	4,7%	1,27	-25,8	0,7278	0,0038	2550	40
AT2007/01 200-260 3-4	203.5	0,5	Bulk sediment	5,6%	1,22	-25,2	0,7944	0,0034	1850	30
AT2007/01 200-260 22-23	222.5	0,5	Bulk sediment	6,2%	1,04	-24,1	0,7546	0,0027	2260	30
AT 2007(100-200 cm) 10-14	112	2	2 large seeds	44,5%	1,061	-10,1	0,8797	0,0016	1030	15
AT 2007(100-200 cm) 55-60	157.5	2,5	192 seeds	41,0%	0,300	-19,6	0,8988	0,0017	855	15

AT 2007(100-200 cm) 80-95	187.5	7,5	245 seeds	41,3%	0,395	-20,1	0,8935	0,0020	905	20
AT 2007(200-260 cm) 6-17	211.5	5,5	2 large seeds	42,6%	1,061	-12,1	0,8745	0,0016	1075	15
AT 2007(200-260 cm) 28-35	231.5	3,5	3 large seeds	53,4%	1,207	-10,8	0,8650	0,0170	1165	15
AT 2007(200-260 cm) 28-48	238	10	240 seeds	17,4%	0,231	-20,6	0,8665	0,0018	1150	15

9. Figure Caption

Figure 1. The Eastern North Anatolian Fault and its associated paleoseismological records (1 for: Fraser *et al.* (2010); 2 for: Zabci *et al.* (2011); 3 for: Fraser *et al.* (This volume); 4 for: Hartleb *et al.* (2006) and Kozaci *et al.* (2011)). The different color underlying the main fault trace show the fault rupture associated with the 1939 M=7.9 Erzincan Earthquake, the 1942 M=7.1 Niksar-Erbaa Earthquake and the eastern part of the 1943 M=7.3 Tosya Earthquake. Our study focuses on the Asacitepecik Lake (AT Lake).

Figure 2. Relationship between the AT Lake and the NAF. The small depression filled by the AT Lake is located along a small releasing step along the NAF, an additional restraining bend and the associated ridge is located to the SE of the AT Lake. Paleoseismological sites are indicated with red diamonds, 1 for: Okomura *et al.* (1994) 2 for: Zabci *et al.* (2008); 3 for: Fraser *et al.* (This volume).

Figure 3. Bathymetry of the AT Lake and the core locations (squares). Continuous red lines indicate fault scarps visible in the seismic lines or in the paleoseismic trench (circle), dash red lines indicate the inferred fault geometry. Lake bathymetry was measured in July 2006 with a sonar GPS. A small village was built along the southern shore of the lake. The lake is in continuity with the flood-plain of the Cobali river (see Figure 2).

Figure 4. Typical seismic line of across the AT Lake obtained using the Innomar Profiler. The upper figure is the Low Frequency signal (6 to 12 kHz) and the lower inset is the High Frequency signal (100 kHz). Small fault scarps are still visible in the central part of the Lake,

and on its southern margin. Surface fault scarps are 10 to 20 cm high, but fault offsets increase at depth.

Figure 5. Correlations between the AT003, AT2007-SC and AT2007 cores. The AT003 gravity core was taken in 2006 in a slightly deeper environment than the AT2007-SC and AT2007. AT2007-SC is a short gravity core taken at the same spot as AT2007, a longer piston core. Only part of the 2.5 m long AT2007 is displayed in this figure. Stratigraphic column, RGB image and X-Ray Scopix pictures with Magnetic susceptibility are indicated. Correlation is based on two main whitish key layers outlined by grey bands, and on magnetic susceptibility data. The stratigraphy of all cores is composed of repeated sedimentary sequences comprising three distinct units. Units 1 are light brown and whitish sandy silty clay units that are very disturbed. Units 2 are disturbed fibrous silty clay units with organic fibers organized in lamina. Units 3 are mostly dark fibrous silty clay unit (fibers have a vertical orientation).

Figure 6. Granulometry of core AT2007-SC. The stratigraphic log is displayed on the left and percentage of clay, silt, and sand particles on the right. Photos of the top of units 1 in sequences 1 and 2 are shown on the right, with their vertical scale. Stars indicated location of sived samples presented in Figure 7.

Figure 7. Content of core AT2007-SC: photographs of the different sedimentary fractions after wet sieving; fractions sampled are indicated with a star in Figure 6. **In a**, the fraction of the sample at the top of unit1-sequence 1 larger than 450 μm is secondary and contains few large seeds and phytoclasts; the main 250-450μm fraction shows an abundance of ostracods and phragmite seeds; the 100-250 μm fraction shows mostly broken ostracods, with some

amorphous silty-clay aggregates. **In b**, the fraction of the sample in unit 1-sequence 1 larger than 450 μm is more abundant with large seeds, some chironomids, different types of plant remains; the 250-450 μm fraction shows a mixture of broken ostracod shells, chironomids, seeds, phytoclasts, amorphous silty-clay aggregates; the 100-250 μm fraction shows broken ostracoda but in less amount than above and amorphous silty-clay aggregates. **In c**, the sediment of unit 3-sequence 2 is dominated by the >450 μm fraction, composed of phytoclasts and fibrous plant remains mostly phragmite (right) and silty-clay aggregates (left).

Figure 8. Analysis of core AT2007 comprising from left to XRD mineralogical change with iron oxide, hydromagnesite and quartz+plagioclase (quantification excluding clay minerals), magnetic susceptibility data and XRF data with Ca and Ti intensity as well Ca/Ti ratio.

Figure 9a. Analyses of the organic matter contained in the AT 2007 cores combining LOI (550oC), $\delta^{13}C$, TOC, C/N ratio and $\delta^{15}N$ measurements (from left to right). To the left is also shown the stratigaphic division of core AT2007 in sequences and units.

Figure 9b. The bottom event in core AT2007 imagery, X-Ray pictures and from left to right: Fe and Ca intensities, magnetic susceptibility measurements, Total Organic Carbon, relative aboundance of goethite and hydromagnesite in a quantification including quartz, plagioclase, clay, calcite, dolomite, hydromagnesite, hematite and goethite.

Figure 10. A modified OxCal (Bronk Ramsey, 2007) plot of the calibrated sample age probability distribution functions (PDFs) (grey), modeled sample age PDFs (no fill black boundary), and earthquake age PDFs (black filled). Samples were calibrated using the InCal04 curve (Reimer *et al.,* 2004).

11. Appendixes

XRD Mineralogy of core AT2007.

Depth (cm)	Quartz	Calcite	Dolomite	Clay	Plagioclase	Hematite	Goethite	Hydro-magnesite
14,5	7%	10%	7%	50%	5%	5%	13%	4%
19,5	6%	8%	7%	48%	6%	6%	15%	4%
23	4%	9%	6%	54%	5%	6%	12%	5%
24	3%	9%	5%	48%	13%	4%	13%	4%
24,5	4%	10%	8%	46%	6%	4%	17%	5%
25	4%	7%	10%	44%	0%	5%	22%	8%
25,5	4%	5%	10%	51%	5%	5%	13%	7%
27	4%	9%	6%	51%	4%	4%	16%	4%
27,5	6%	8%	5%	49%	7%	7%	14%	4%
28	1%	7%	9%	41%	17%	6%	14%	5%
28,5	4%	4%	9%	50%	8%	6%	13%	6%
29	4%	5%	8%	53%	0%	5%	17%	8%
29,5	3%	3%	7%	49%	6%	5%	18%	8%
30	5%	6%	6%	61%	0%	4%	12%	5%
30,5	3%	6%	5%	51%	6%	5%	19%	5%
31,5	4%	5%	6%	54%	5%	5%	13%	7%
32	4%	5%	8%	52%	0%	4%	18%	9%
32,5	4%	5%	8%	46%	4%	6%	20%	7%
33,5	4%	7%	4%	54%	7%	6%	16%	2%
35	3%	8%	9%	44%	5%	4%	17%	9%
37	5%	10%	8%	50%	4%	3%	14%	5%
41,5	5%	8%	6%	60%	0%	4%	13%	4%
46,5	4%	6%	6%	55%	5%	4%	14%	6%
50	7%	9%	6%	51%	5%	5%	12%	4%
55,5	5%	7%	6%	53%	6%	4%	13%	6%
59,5	4%	6%	8%	50%	0%	4%	20%	8%
60,5	5%	7%	9%	50%	0%	6%	15%	8%
62,5	4%	6%	9%	42%	4%	8%	16%	10%
63,5	3%	3%	9%	41%	5%	8%	18%	13%
64,5	2%	6%	8%	51%	5%	4%	15%	9%
67	3%	5%	8%	49%	0%	6%	17%	11%
67,5	2%	4%	5%	59%	5%	4%	14%	8%
68,5	4%	5%	8%	46%	6%	6%	15%	10%
69,5	3%	5%	6%	52%	5%	6%	16%	7%
74,5	4%	6%	7%	48%	5%	6%	17%	7%
79,5	6%	5%	6%	47%	5%	6%	18%	6%
81,5	8%	5%	6%	53%	6%	5%	14%	4%
86	5%	7%	9%	43%	4%	9%	16%	7%
88	4%	6%	8%	47%	6%	4%	17%	7%
95,5	5%	7%	7%	53%	6%	5%	12%	5%
99,5	5%	6%	8%	56%	5%	5%	14%	2%
100,5	2%	2%	6%	52%	5%	4%	21%	7%

101,5	3%	6%	5%	53%	3%	0%	22%	7%
104,5	4%	8%	9%	47%	6%	8%	18%	0%
107,5	4%	6%	9%	51%	5%	3%	17%	5%
109,5	5%	6%	8%	52%	6%	5%	17%	0%
112,5	3%	7%	6%	49%	3%	4%	19%	9%
114,5	5%	7%	10%	46%	5%	4%	16%	6%
115,5	2%	6%	9%	52%	5%	4%	11%	10%
117,5	3%	5%	9%	56%	5%	6%	10%	9%
120,5	2%	8%	8%	45%	6%	8%	18%	6%
123,5	6%	7%	7%	54%	5%	4%	14%	5%
126,5	4%	6%	7%	51%	4%	7%	14%	7%
129,5	4%	5%	7%	46%	5%	4%	22%	8%
132,5	5%	6%	7%	47%	6%	5%	17%	7%
139,5	5%	7%	6%	52%	5%	5%	15%	6%
144,5	5%	7%	7%	54%	4%	5%	13%	5%
149,5	5%	5%	7%	57%	0%	4%	16%	5%
154,5	6%	8%	6%	54%	6%	5%	12%	5%
159,5	6%	7%	6%	58%	6%	4%	10%	3%
162,5	7%	8%	6%	55%	6%	4%	11%	3%
170,5	6%	7%	5%	59%	6%	3%	11%	2%
174,5	6%	7%	5%	61%	6%	4%	9%	2%
179,5	8%	9%	7%	53%	6%	3%	12%	3%
189,5	6%	10%	7%	55%	7%	4%	10%	3%
194,5	9%	7%	6%	52%	10%	4%	11%	0%
199,5	6%	6%	7%	57%	7%	3%	12%	2%
204,5	8%	7%	6%	66%	7%	2%	0%	2%
206,5	7%	10%	6%	68%	6%	3%	0%	0%
208,5	5%	5%	8%	55%	5%	4%	14%	5%
212,5	4%	5%	9%	49%	5%	5%	17%	8%
214,5	5%	7%	9%	50%	5%	4%	15%	6%
216,5	5%	8%	8%	55%	6%	3%	10%	5%
227,5	6%	8%	8%	61%	6%	3%	9%	0%
230,5	1%	9%	6%	51%	12%	6%	15%	0%
234,5	7%	11%	6%	58%	7%	2%	10%	0%
239,5	7%	11%	5%	70%	8%	0%	0%	0%

Figure 1

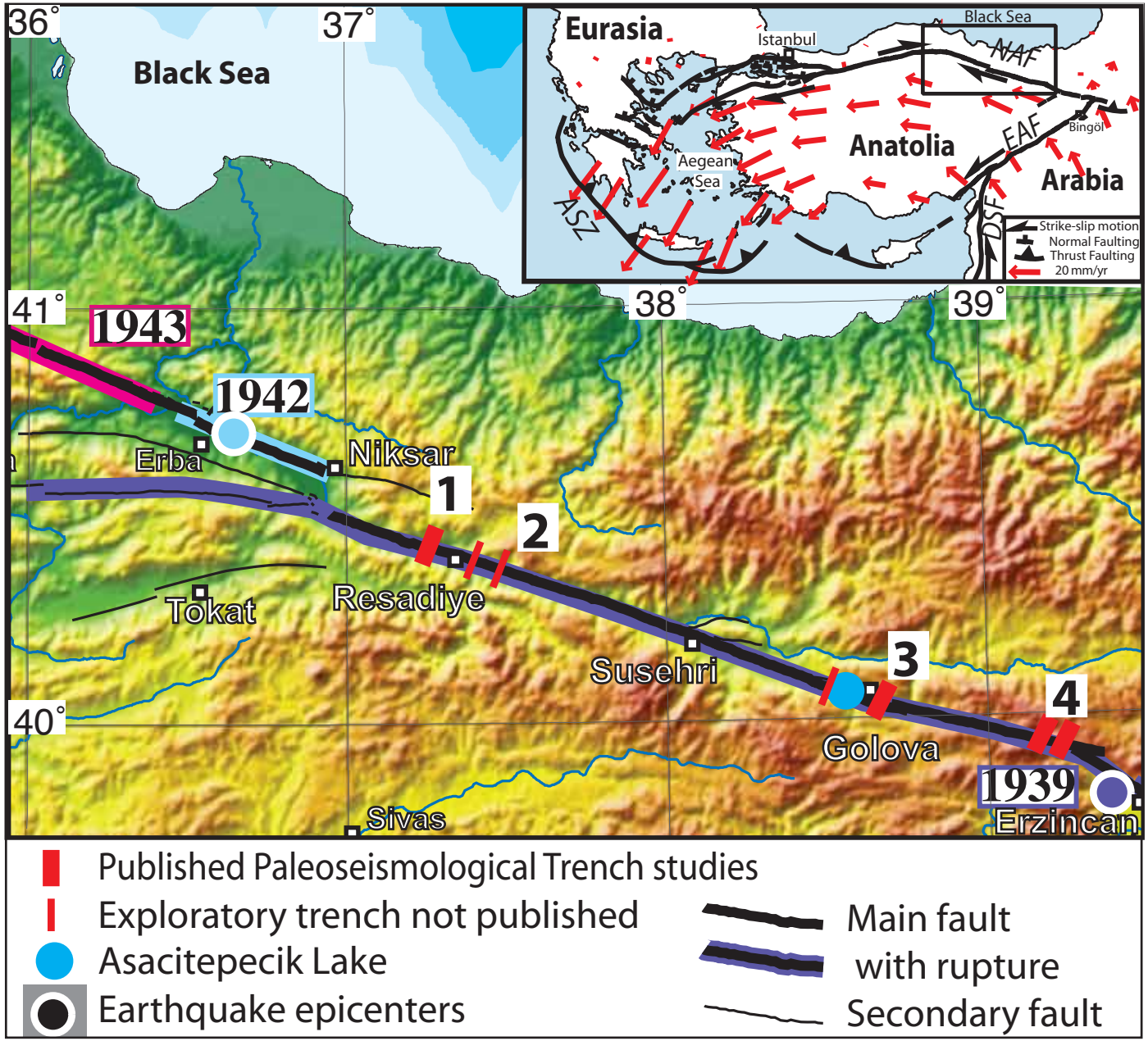
36°
37°
38°
39°
41°
40°
Black Sea
1943
1942
Erba
Niksar
1
2
Tokat
Resadiye
Susehri
3
4
Golova
1939
Erzincan
Sivas
Eurasia
Istanbul
Black Sea
NAF
EAF
Bingöl
Anatolia
Aegean Sea
Arabia
ASZ
DSF
Strike-slip motion
Normal Faulting
Thrust Faulting
20 mm/yr
Published Paleoseismological Trench studies
Exploratory trench not published
Asacitepecik Lake
Earthquake epicenters
Main fault
with rupture
Secondary fault

Figure 2


E38°34′30′
E38°37′30′
N40°03′
N40°01′
Golova Dam Lake
Asacitepecik Lake
Cobanli R.
Cobanli River
Gunulan Village
1
2
3
4
+
-
1500 m

Figure 3

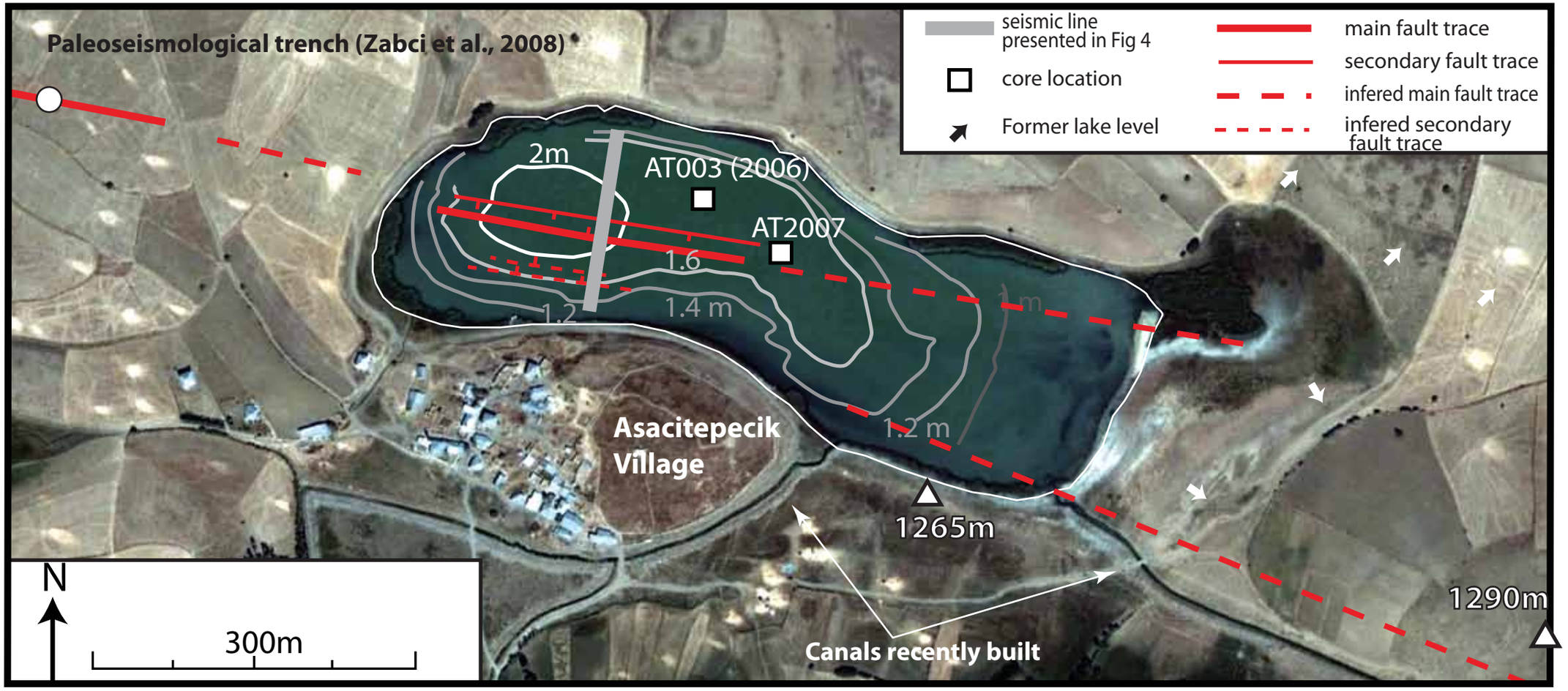
Paleoseismological trench (Zabci et al., 2008)
seismic line presented in Fig 4
core location
Former lake level
main fault trace
secondary fault trace
infered main fault trace
infered secondary fault trace
2m
AT003 (2006)
AT2007
1.6
1.4 m
1.2
1 m
1.2 m
Asacitepecik Village
1265m
1290m
Canals recently built
N
300m

Figure 4

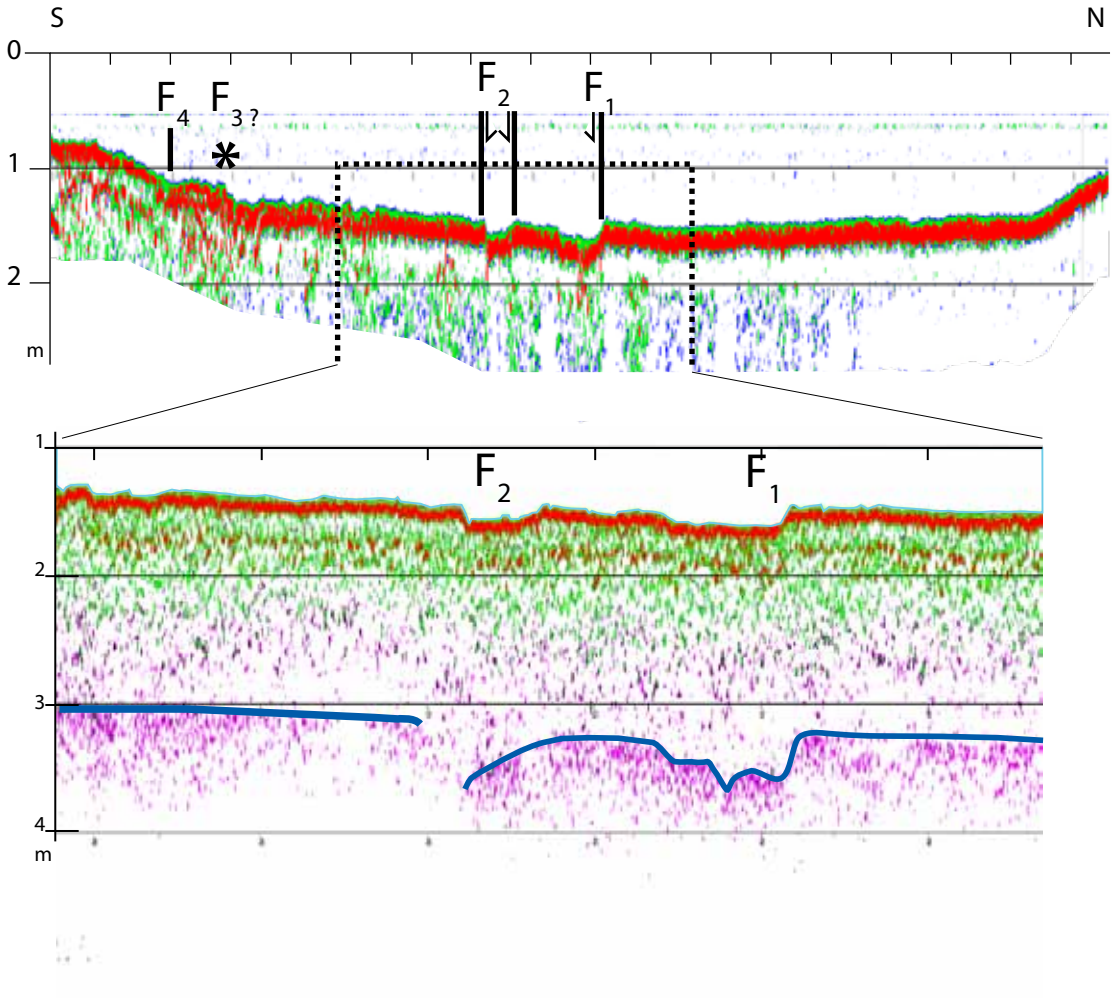

Figure 5

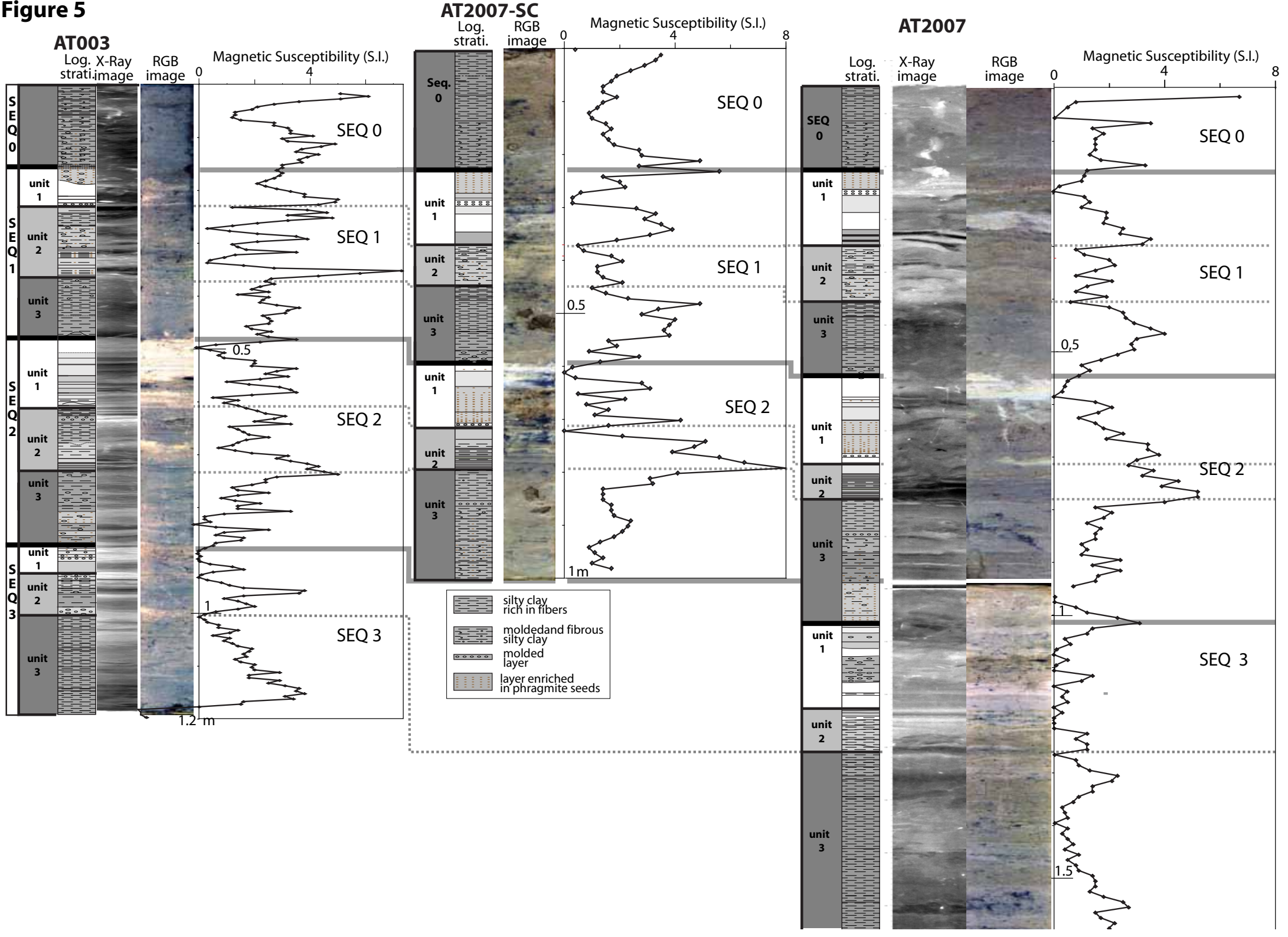
AT003
Log. strati.
X-Ray image
RGB image
Magnetic Susceptibility (S.I.)
0
4
SEQ 0
unit 1
SEQ 1
unit 2
unit 3
0.5
SEQ 2
unit 1
unit 2
unit 3
1
SEQ 3
unit 1
unit 2
unit 3
1.2 m
AT2007-SC
Log. strati.
RGB image
Magnetic Susceptibility (S.I.)
0
4
8
Seq. 0
unit 1
unit 2
unit 3
unit 1
unit 2
unit 3
SEQ 0
SEQ 1
0.5
SEQ 2
1m
silty clay rich in fibers
moldedand fibrous silty clay
molded layer
layer enriched in phragmite seeds
AT2007
Log. strati.
X-Ray image
RGB image
Magnetic Susceptibility (S.I.)
0
4
8
SEQ 0
unit 1
unit 2
unit 3
unit 1
unit 2
unit 3
unit 1
unit 2
unit 3
SEQ 0
SEQ 1
0,5
SEQ 2
1
SEQ 3
1.5

Figure 6

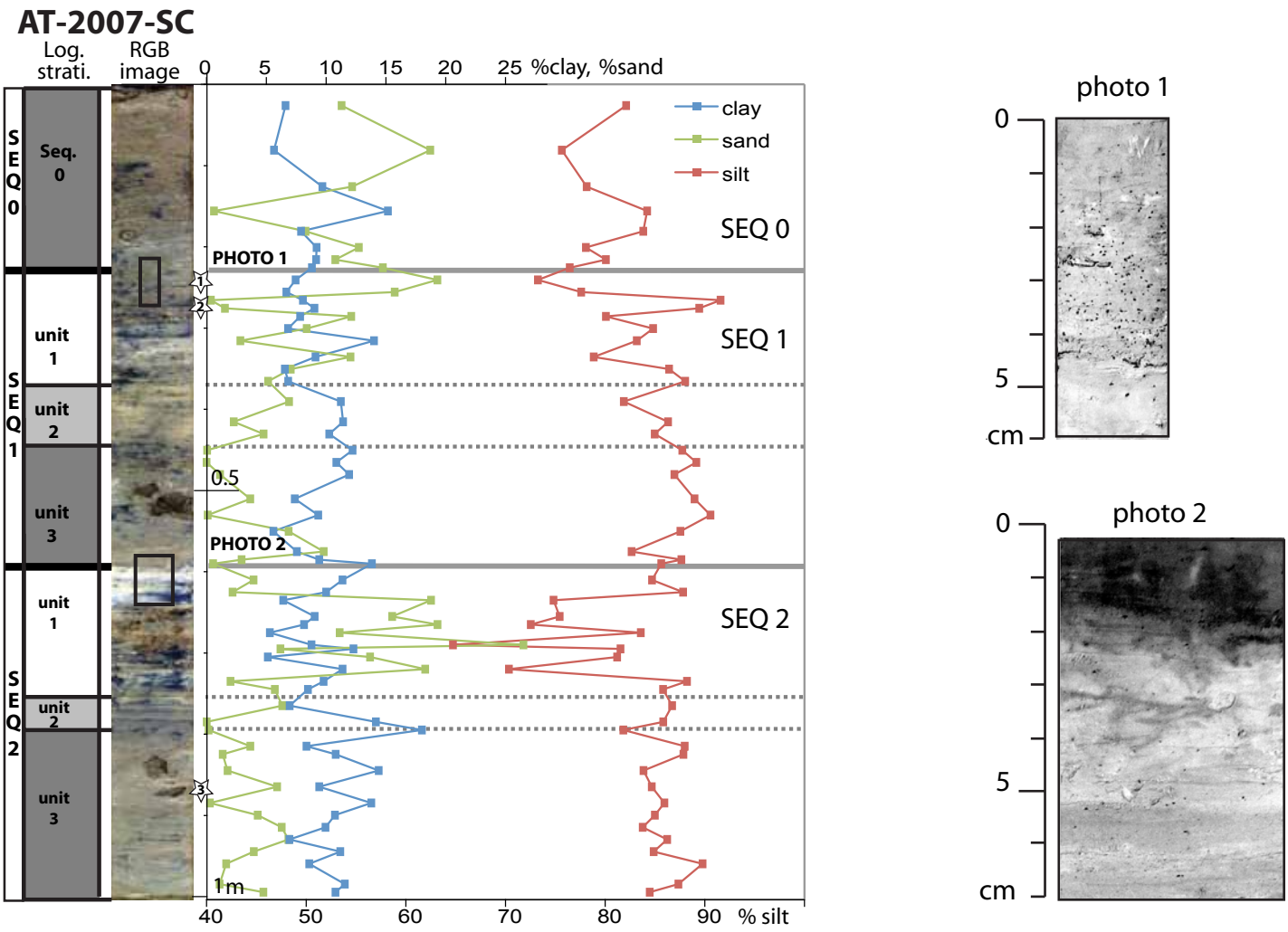
AT-2007-SC
Log. strati.
RGB image
0 5 10 15 20 25 %clay, %sand
clay
sand
silt
SEQ 0
SEQ 1
SEQ 2
Seq. 0
unit 1
unit 2
unit 3
unit 1
unit 2
unit 3
PHOTO 1
PHOTO 2
0.5
1m
40 50 60 70 80 90 % silt
photo 1
0
5
cm
photo 2
0
5
cm

Figure 7

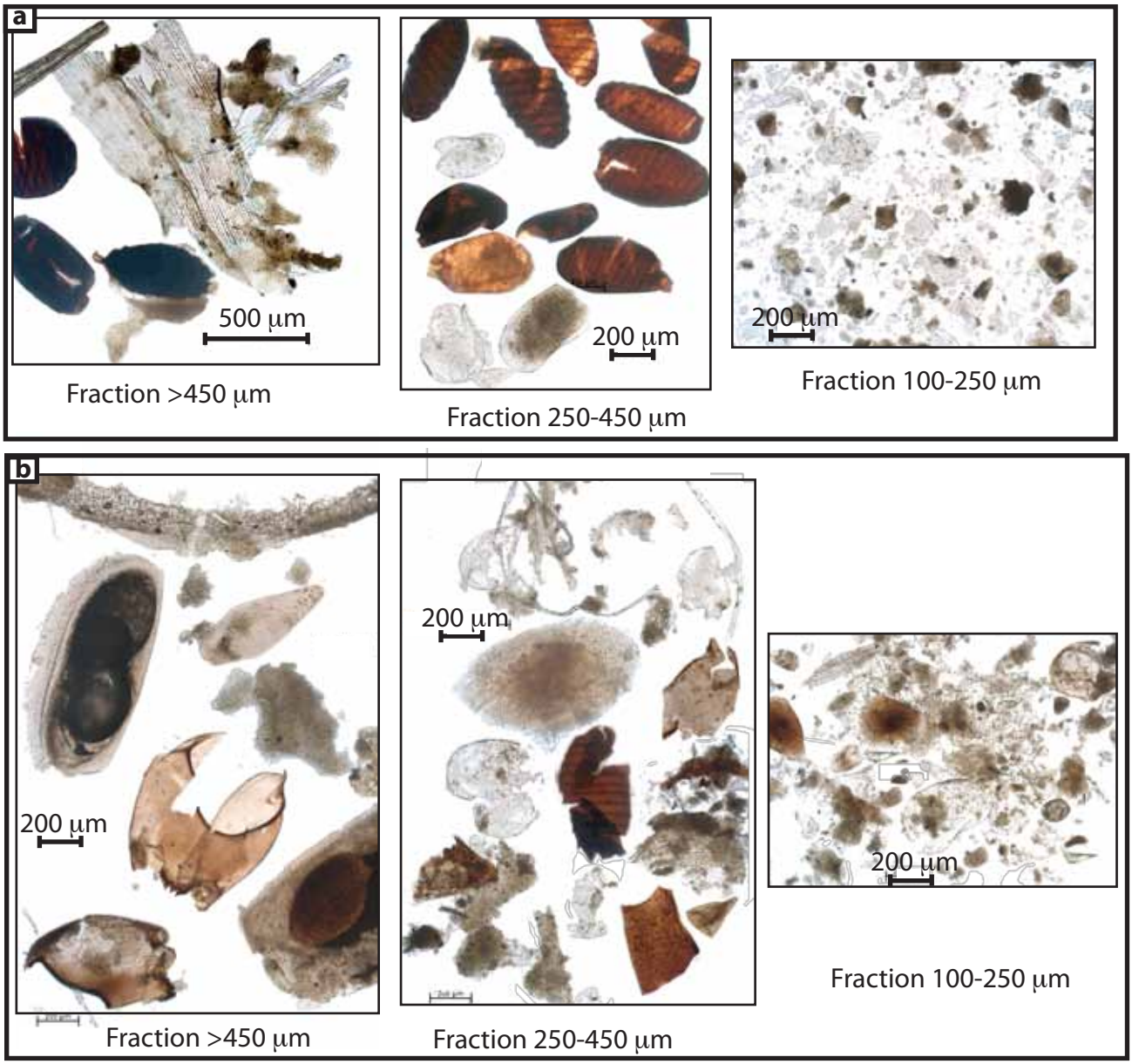
a
500 µm
Fraction >450 µm
200 µm
Fraction 250-450 µm
200 µm
Fraction 100-250 µm
b
200 µm
Fraction >450 µm
200 µm
Fraction 250-450 µm
200 µm
Fraction 100-250 µm
c
200 µm
200 µm
Fraction >450 µm

Figure 8

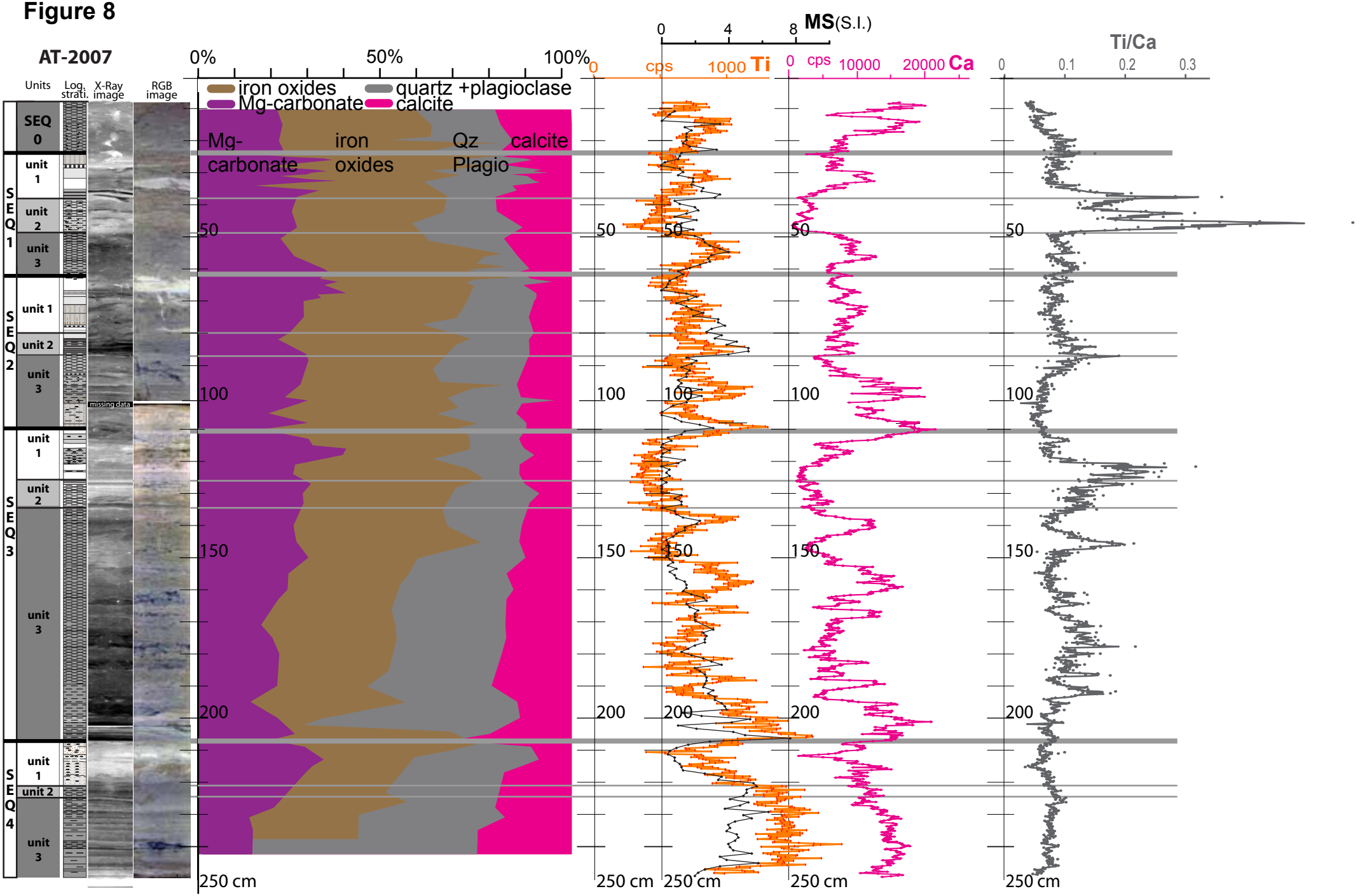
AT-2007
Units
Log. strati.
X-Ray image
RGB image
0%
50%
100%
iron oxides
quartz +plagioclase
Mg-carbonate
calcite
Mg-carbonate
iron oxides
Qz
Plagio
calcite
MS(S.I.)
0
4
8
Ti
cps
1000
Ca
10000
20000
Ti/Ca
0.1
0.2
0.3
SEQ 0
SEQ 1
unit 1
unit 2
unit 3
SEQ 2
unit 1
unit 2
unit 3
missing data
SEQ 3
unit 1
unit 2
unit 3
SEQ 4
unit 1
unit 2
unit 3
50
100
150
200
250 cm

Figure 9a

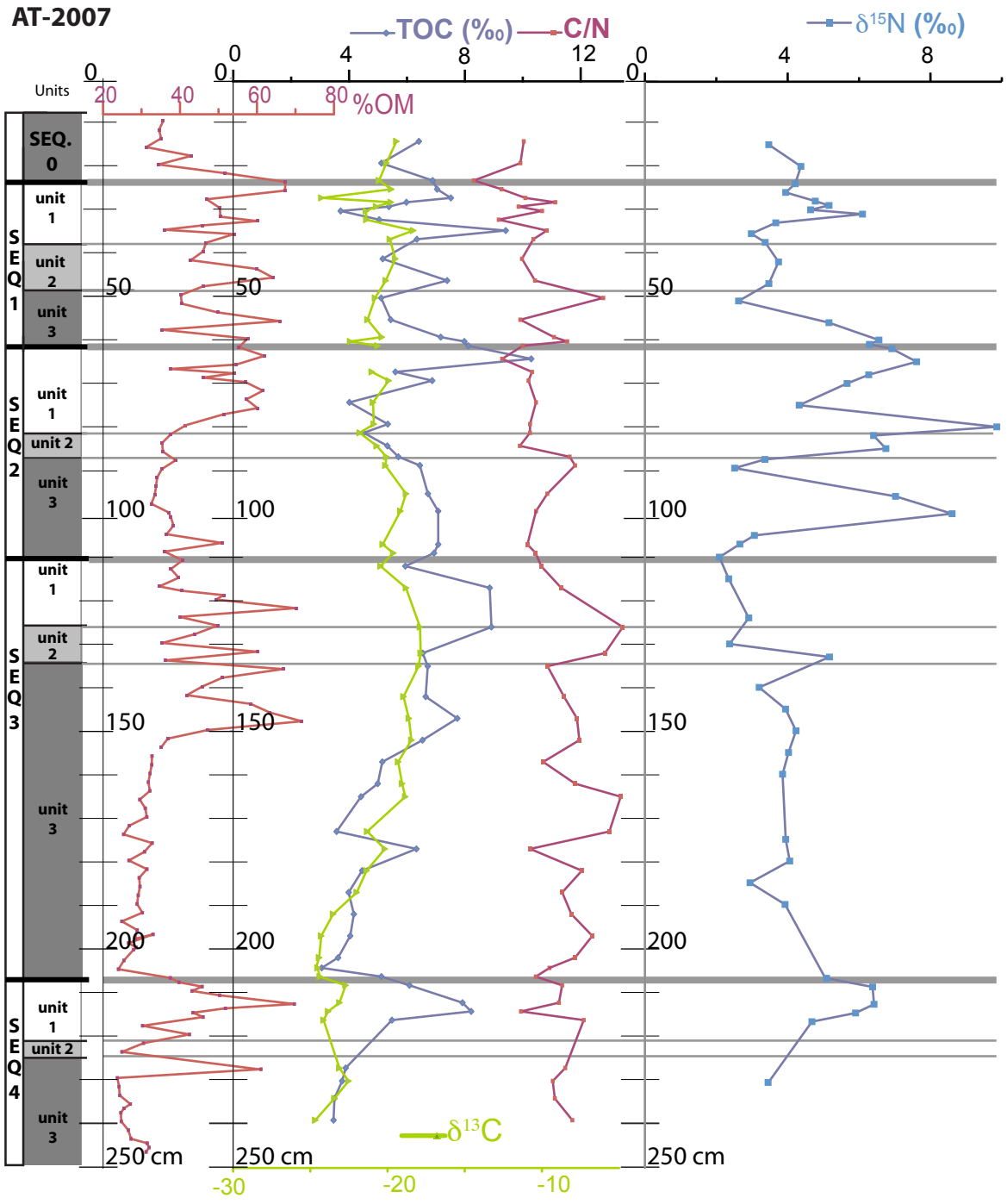
AT-2007
TOC (‰)
C/N
δ15N (‰)
%OM
Units
SEQ. 0
SEQ 1
SEQ 2
SEQ 3
SEQ 4
unit 1
unit 2
unit 3
δ13C
250 cm

Figure 9b

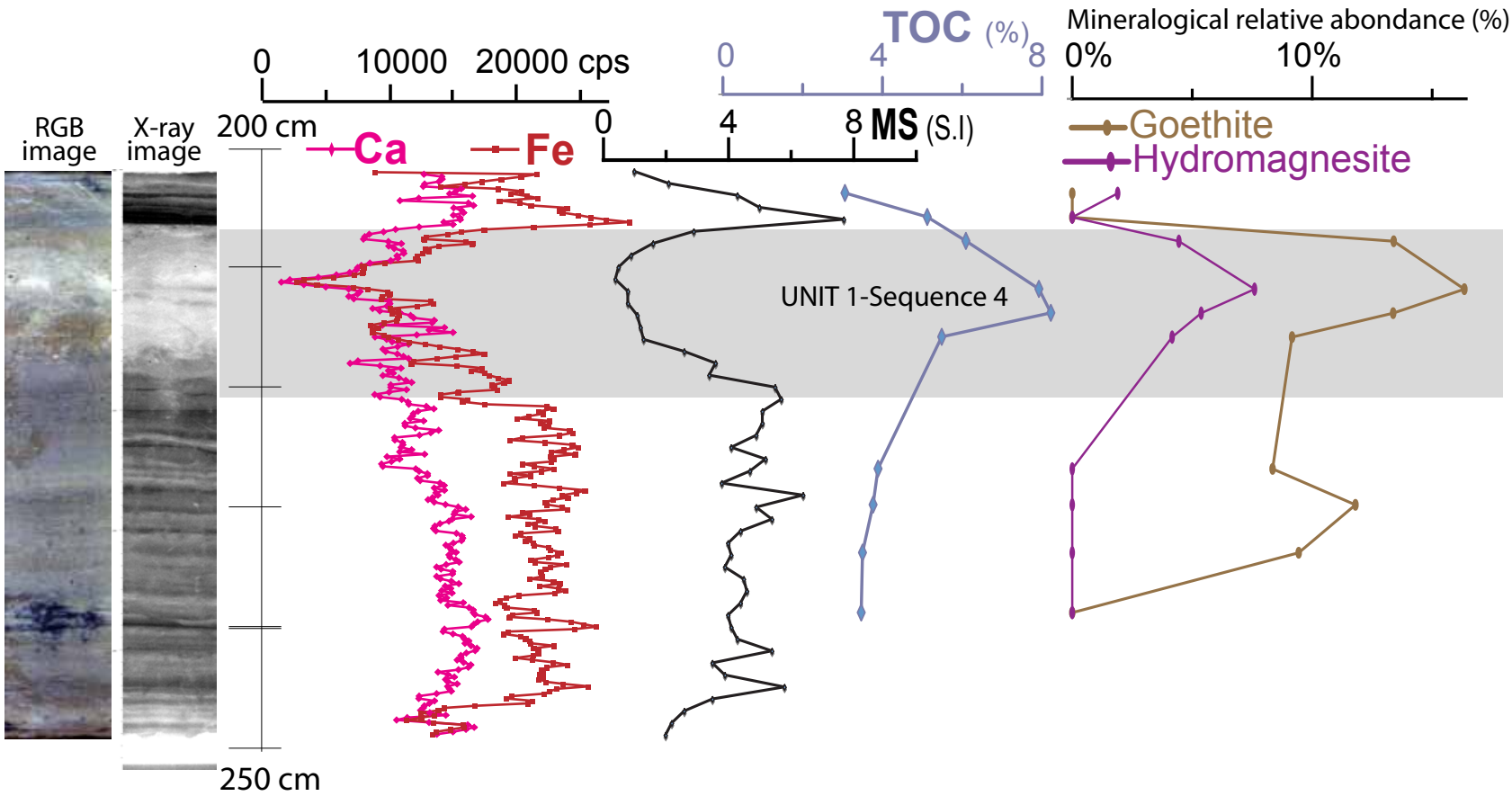
RGB image
X-ray image
200 cm
250 cm
0
10000
20000 cps
Ca
Fe
TOC (%)
0
4
8
0
4
8 MS (S.I)
Mineralogical relative abondance (%)
0%
10%
Goethite
Hydromagnesite
UNIT 1-Sequence 4

Figure 10

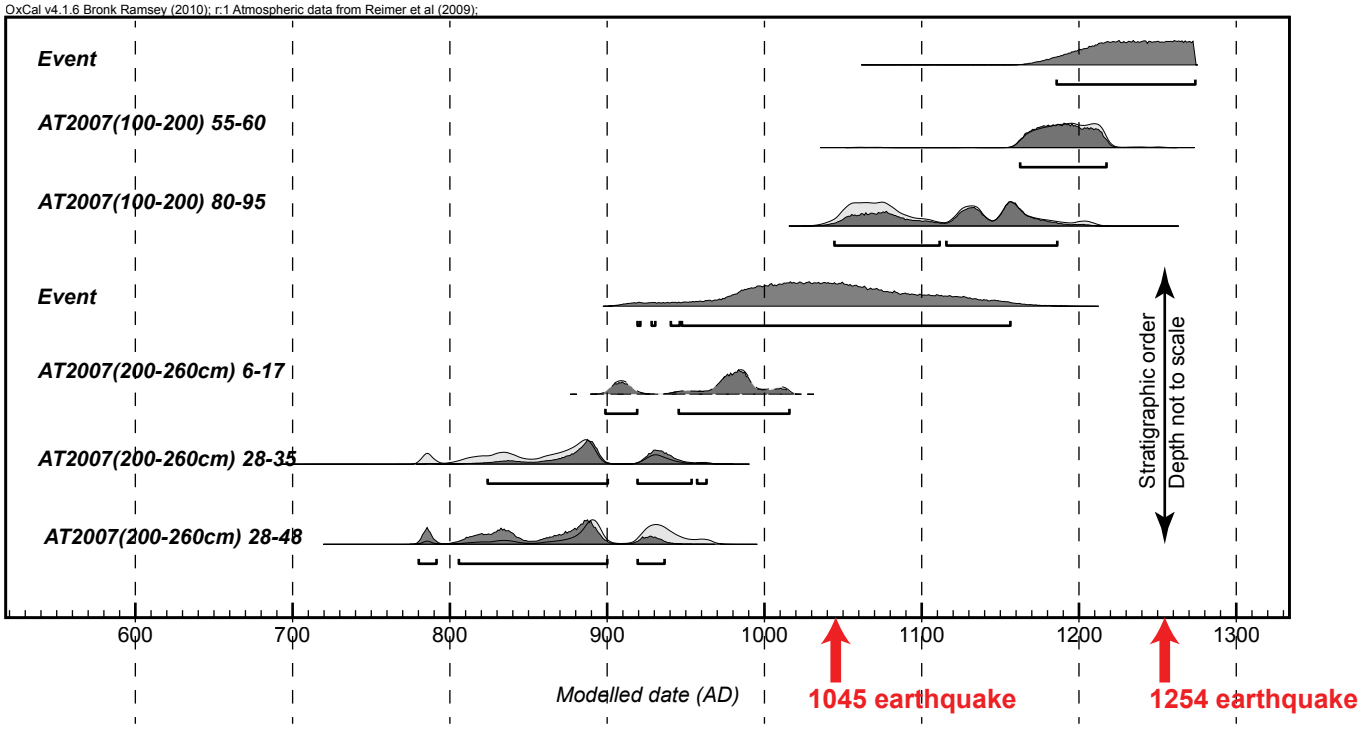
OxCal v4.1.6 Bronk Ramsey (2010); r:1 Atmospheric data from Reimer et al (2009);
Event
AT2007(100-200) 55-60
AT2007(100-200) 80-95
Event
AT2007(200-260cm) 6-17
AT2007(200-260cm) 28-35
AT2007(200-260cm) 28-48
Stratigraphic order
Depth not to scale
600
700
800
900
1000
1100
1200
1300
Modelled date (AD)
1045 earthquake
1254 earthquake